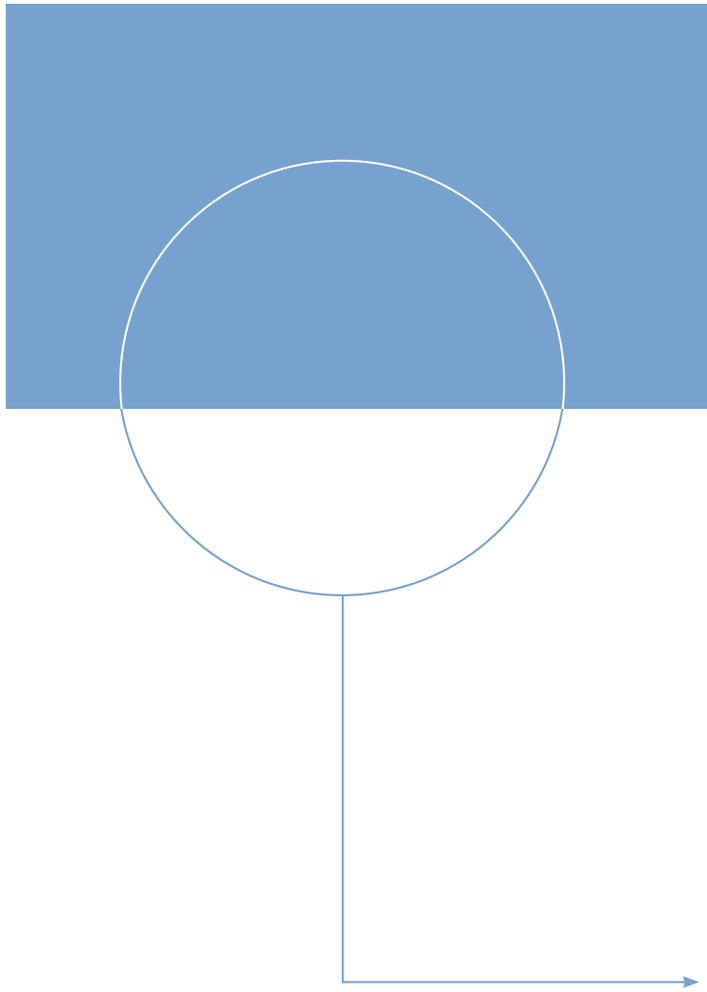

Master's thesis

2022

Patrick R-F Heian Jørgensen

NTNU
Norwegian University of
Science and Technology
Faculty of Engineering
Department of Energy and Process Engineering

Patrick R-F Heian Jørgensen

Photo Ignition of methane air mixtures using carbon nanotubes

June 2022

NTNU
Norwegian University of
Science and Technology

NTNU
Norwegian University of
Science and Technology

NTNU
Norwegian University of
Science and Technology

Photo Ignition of methane air mixtures using carbon nanotubes

Patrick R-F Heian Jørgensen

Energy and process engineering
Submission date: June 2022
Supervisor: David Emberson
Co-supervisor: Karl Oskar Pires Bjørgen

Norwegian University of Science and Technology
Department of Energy and Process Engineering

Abstract

The fuel transition from burning hydrocarbons has become an inevitable reality as the consequences of climate change are evident. Ammonia is forecast to be a major carbon-free fuel in the emission intensive maritime shipping industry, but as a fuel, ammonia comprises undesirable combustion characteristics. One of the possibility to improve these characteristics would be to look at the ignition method. An interesting concept, first demonstrated by Ajayan et al. [1] showed that carbon nanotubes with metal impurities ignites in air when exposed to a camera flash. Berkowitz et al. [2] extended this idea to disperse these particles in a stationary combustion chamber to achieve quasi homogeneous ignition, resulting in an significantly more efficient combustion. There are still research gaps for implementing this concept in an engine cylinder, arguably most importantly would be to achieve the ignition from a remote energy source.

In this thesis the feasibility of constant volume combustion with photo-induced ignition of carbon nanotubes with a remote xenon based flash was investigated. The aim was to analyze different strategies to remotely initiate the combustion process on a methane/air mixture. Before attempting ignition by the xenon flash, the chamber was verified in terms of reliability and correct mixture compositions through data analysis and high speed camera images. Photo-induced ignition on different particle distributions were looked at, where successful ignition of the mixture occurred in a dispersed sample in front of the xenon flash. Ignition was limited to the narrow range of the equivalence ratio from 0.7 to 0.8 at initial pressures from 2 to 4 bar. Moreover, three different amounts of particles were tested and within the aforementioned range all samples ignited the mixture. The flame was filmed for the equivalence ratio on 0.8 and initial pressure at 4 bar, where the flame was dominated by the effects of the burning particles. Observations suggested that for photo-induced ignition on carbon nanotubes, there are an upper and a lower limit for the burning particle density where successful ignition could occur. It was concluded that too dense would consume the local oxygen while creating a relatively large amount smoke, and too spread out would not release enough local heat to initiate the combustion of the mixture.

Sammendrag

Det er bred enighet om at fossile brennstoff må utveksles med karbonfrie alternativer grunnet konsekvensene av klima endringer. Ammoniak er spådd til å være et lovende karbon fritt alternativ for maritime fartøy, men forbrennings egenskapene til ammoniak gjør det til et ikke ideelt drivstoff. En mulighet for å forbedre forbrennings karakteristikken til amoniakk kan være å se på antenningsmetoden. Et interessant konsept, først gjennomført av Ajayan et al. [1] viste at ''carbon nanotubes" med metalliske urenheter tar fyr etter de har blitt utsatt for en kamera blitz. Berkwotz et al. [2] tok dette videre ved å spre disse partiklene homogent i et forbrennings kammer og oppnådde quasi homogen antenning som resulterte i en kraftigere forbrenning. Det er fremdeles en lang vei å gå før denne metoden er gjennomførbar i en motor sylinder, diskuterbart vil det å oppnå dette fra en ekstern kilde være noe av det viktigste.

I denne oppgaven ble gjennomførbarheten av konstant volum forbrenning med foto-indusert antenning av ''carbon nanotubes", aktivert med en ekstern kilde undersøkt. Målet var å analysere ulike strategier for å eksternt aktivere en forbrenningsprosess av en metan/luft blanding. Før foto-indusert antenning ble gjennomført, så var forbrennings kammeret verifisert i form av pålitelighet og korrekt blandingsforhold. Dette ble gjort via data analyse og høy hastighets bilder. Foto-indusert antenning på ulike partikkel distribusjoner ble sett på, hvor suksessfull antenning skjedde ved en spredt distribusjon rett foran xenon lampen. Antenningen var begrenset innenfor et lite intervall av ekvivalens ratioen fra 0.7 til 0.8 ved trykk mellom 2 og 4 bar. Tre ulike mengder med nanopartikler ble undersøkt, der samtlige antente blandingen innenfor de nevnte intervallene. Flammen skapt av denne antenningsmetoden ble filmet ved ekvivalens ratio på 0.8 og trykk ved 4 bar. Flammen var dominert av effektene skapt av de brennene partiklene og var helt forskjellig fra tennplugg antenning. Observasjonene gjort foreslår at det finnes en øvre og en nedre grense for partikkel tettheten, der suksessfull antenning kan skje. For tett og partiklene vil konsumere det lokale oksygeninnholdet og skape relative store mengder røyk rundt flammen. For lite og partiklene frigjør ikke nok energi til å aktivere forbrenningen.

Acknowledgements

I would like to thank my supervisors, Karl Oskar Pires Bjørgen, David Emberson and Therese Løvås for their continuous guidance through the project and master thesis. A special thanks to Karl Oskar for his cooperation and guidance, making the countless hours at the lab facility both safe and enjoyable. I would also like to thank The Norwegian University of Science and Technology (NTNU) and SINTEF for lending the lab facilities and always supporting with the necessary equipment so I could focus on the research. Thanks to Stian Ranøyen Bratsberg for discussing concepts and ideas, providing valuable insights. I would also like to thank my mother Hanne Edel Jørgensen for her continuous support throughout my entire degree, without her none of this would have been possible. Finally, I would like to thank my partner Hanna Sørheim for moral support, taking care of our business while I was away studying and for reading through my work, advising me on language and writing techniques.

Table of Contents

List of Figures

List of Tables

Abbreviations

IMO - International Maritime Organization

GHG - Green House Gases

SI - Spark-induced Ignition

CI - Compression Ignition

HCCI - Homogeneous Charge Compression Ignition

CNT - Carbon Nanotubes

SWCNT - Single Walled Carbon Nanotubes

MWCNT - Multi Walled Carbon Nanotubes

PI - Photo-induced Ignition

CVCC - Constant Volume Combustion Chamber

NTNU - Norwegian University of Science and Technology

P&ID - Process and Instrument Diagram

Synair - Synthetic air

FAR - Fuel to Air Ratio

MIE - Minimum Ignition Energy

PRV - Pressure Relief Valve

HEPA - High Efficiency Particulate Air

TDMS - Technical Data Management Streaming

fps - Frames Per Seconds

Nomenclature

Chemical symbols

N_2	Nitrogen
C	Carbon
C_xH_y	Arbitrary hydrocarbon
CH_4	Methane
CO	Carbon Monoxide
CO_2	Carbon dioxide
Fe	Iron
Fe_xO_y	Arbitrary Iron oxide
NH_3	Ammonia
NO_x	Nitric Oxides
O2	Oxygen
Xe	Xenon

Physics constants

$\bar{R}$	Universal gas constant

Variables

$\bar{x}$	Generic mean
Δp	Pressure difference between chamber and injection line
$\frac{dp}{dt}$	Pressure gradient
ϕ	Equivalence ratio
ϕ_T	Targeted equivalence ratio
dp_{max}	Maximum pressure gradient during combustion

FAR	Fuel to air ratio
m_{CNT}	Mass of CNT/Fe mix
N	Sample size
n	Amount of mole
p	Pressure
p_a	Initial air pressure
p_t	Pressure at combustion trigger
p_{peak}	Peak combustion pressure
Q	Heat
T	Temperature
T_a	Initial air temperature
t_f	Flash trigger time
T_t	Temperature at combustion trigger
t_{0-1}	Chamber air filling time
t_{1-2}	Time between process 1 and 2
t_{2-3}	CH_4 filling time
t_{ds}	Turbulence dissipation time
t_{mix}	Gas mixing time
V	Chamber volume
V_{CNT}	CNT module volume
V_{ig}	Injection gas volume
x_i	Generic ith sample in a series
Z	Compressibility factor
z	Stoichiometric coefficient

Chapter 1

Introduction

1.1 Background

The Paris Agreement on climate change signed in 2015 at the Conference of Parties 21 stated the urgency to strengthen the global response towards climate change. The goal was to ensure that the global average temperature would not surpass 2 °C and to pursue efforts to limit temperature increase to 1.5 °C [Paris Agreement]. However, the Emissions Gap Report in 2021 by the United Nations Environment Programme stated that the world is on track to a 2.7 °C by the end of the century at the current pace [3]. One of the sectors that contribute largely towards climate change is the maritime sector, contributing with 2.89% of global anthropogenic carbon dioxide (CO_2) emissions in 2018 [4]. The International Maritime Organization (IMO) found that this is an increase of 9.3% compared to 2012 and they project the emissions to grow another 40% by 2050. IMO has agreed to aim at a 50% greenhouse gas (GHG) reduction in 2050 compared to 2008 and at least a 70% reduction in carbon intensity within the same time frame. These ambitious goals incentives fuel transition and fuel efficiency of large maritime vessels as hydrocarbon combustion with traditional spark-plug or compression ignition is the current standard.

Alternative low carbon fuels for maritime applications are being developed with promising results. Liquefied natural gas, methanol, dimethyl ether, ethanol and biodiesel are examples of viable fuels in terms of performance and feasibility, but they are merely a temporarily solution to the long term zero emission goal. Another promising fuel is ammonia (NH_3) which has recently attracted a great deal of international attention, being forecast as a major fuel for maritime applications. NH_3 could potentially be a carbon free fuel and has the benefits of developed infrastructure, established transport networks and flexibility in terms of both storage and usage. However, NH_3 comprises its own set of challenges such as low flame speed, narrow flammability limit and production of nitric oxides (NO_x). These are all undesirable combustion characteristics and ammonia by itself is therefore not a viable option yet with respect to performance.

There are ways to improve combustion performance by for example optimizing fuel composition, premixing, increasing compression ratios and looking at the ignition

method itself in terms of method and timing. The two major ignition methods are Spark-induced Ignition (SI) and Compression Ignition (CI). While SI utilizes a premixed charge, it is a point ignition method where the flame develops from a single point. Premixing provides a homogeneous mixture composition, but limits compression ratios as the mixture can spontaneously ignite during the compression stroke and ultimately damage the engine. CI allows for greater compression ratios and therefore greater motor efficiency as the fuel is injected at the end of the compression stroke. Since this method relies on the auto ignition temperature, the temperature where the fuel react spontaneously, ignition can occur in several places at the same time. A down sight is that the fuel and air react before being able to mix fully. A third ignition method called Homogeneous Charge Compression Ignition (HCCI) takes the premixing from SI and the high compression ratios from CI, resulting in superior fuel economy and ultra low NO_x and particle matter emissions. [5] This method is in practical terms decoupled from a direct ignition trigger such as the spark-plug or the fuel-spray. Without effective strategies to control the auto-ignition timing on time according to the operating conditions, the HCCI engine will be limited in a small operation range due to problems with cold starts, combustion noise and even uncontrolled spontaneous combustion at high loads.

A promising, yet new method that could lead to homogeneous ignition is the utilization of the thermal properties of Carbon Nanotubes (CNT). It has been shown that by adding metallic particles to the nano structure and exposing the sample to a low energy light sources, the particles are able to ignite and release heat. A concept where particles are dispersed homogeneously in a motor cylinder and triggered by Photo-induced Ignition (PI) at an optimal timing, could lead to increased performance as well as acting as an ignition trigger for effective ignition timing. However, the concept is relatively new and requires further research.

1.2 Objective

This project fits into a larger project that aims to create an optical accessible engine fueled by NH_3. In that regard, this thesis was aimed to take the first steps to investigate PI of CNTs as a potential ignition method. Due to the potential to have a premixed charge with multiple ignition points, the idea was that this ignition method could enhance the many unfavorable characteristics of NH_3/air mixtures. Therefore, the vision for this thesis was to successfully ignite a combustible mixture in a Constant Volume Combustion Chamber (CVCC) by PI of CNTs with an external light source.

To the best of this authors knowledge, this has not been accomplished before, but would be a leap towards integrating the method in motor applications where internal light sources are not feasible. Working towards that goal the objectives were two sided, first focusing on SI to verify reliable operation of the CVCC and the other investigating the limits and potential of PI.

For spark induced ignition the objectives were as followed:

- Develop and verify chamber filling procedure to ensure controlled mixture composition
- Develop a mixing mechanism and procedure to ensure a premixed charge
- Perform a combustion study with SI, characterising limitations and performance and build a base case for SI in the CVCC.
- Validate the base case in terms of statistics and high speed camera imaging to existing literature.

For the photo induced ignition the objectives were as followed:

- Develop a CNTs injection system with variable flow characteristics.
- Evaluate the injection jet using high speed camera imaging and suggest an injection strategy.
- Characterise limits of PI and provide a proof of concept for externally based light sources as the ignition trigger in a CVCC.
- Perform a combustion study with PI and compare with the base study for SI in terms of limits and performance.

1.3 Previous work

SINTEF in collaboration with NTNU started the "Nanoignite" project back in 2021. Two test rigs were set up, one with the optical accessible engine and one with the CVCC. The CVCC was set-up and a Process and Instrument Diagram (P&ID) developed. The gas lines were CH_4 and synethetic air (synair) and a control software was made for regulating the solenoid valves. Furthermore, initial testing was done by the author on the project thesis in 2021 [6]. The findings in that thesis showed that the CVCC proved unreliable in terms of combustion characteristic and consistency. Unambiguously, the mixture composition was not that of the target mixture composition with a offset in the range of 20-40%, varying with the pressure. The CVCC had narrow limits where the mixture was able to ignite and combustion characteristics suggested that the mixture was non-premixed to the point where no conclusions could be drawn.

In terms of PI several different light sources have been tested on different CNTs samples in this project [7]. Light emitting diodes and laser diodes did not provide the required activation energy so it was decided to investigate Xenon (Xe) based light sources. Xe based PI has been accomplished in CVCC before, only while mounted internally inside the combustion vessel. [2], [8], [9]

Chapter 2

Theory

The theoretical foundation for this thesis is covered in this chapter. The objective of this thesis was the PI of CNTs, which invoked two key subjects to research. First, a literature survey on the CNT, its thermal properties and usage as an ignition agent was explored. The PI is a new phenomenon, which means that the existing literature is still not conclusive. After exploring the previous work on CNTs the combustion fundamentals used throughout in this thesis are presented. The focus is set around mixture compositions, key combustion parameters, flame characterisation, and the combustion of CH_4/air mixtures.

2.1 The Carbon Nanotube

CNT was first discovered in 1991 and is one of the allotropes of carbon, an intermediate between the caged-like fullerene and flat graphene [10]. The allotrope is shaped as a hollow cylinder with one or multiple graphene sheets rolled together making up the frame in a hexagonal shaped lattice. The nanotubes have a high aspect ratio where the diameter is in the range of nanometers and the length can go up to a micron. CNT is considered the strongest material in nature in terms of tensile strength and the elastic modulus due to the strong covalent sp^2 bonds between the carbon atoms arranged in a seamless hexagonal structure.

CNT is synthesized through the arc discharge method where a direct-current arc voltage is applied between two pure graphite electrodes immersed in an inert gas such as helium and creates CNT in the form of soot. By utilizing two graphite electrodes the process generates multiple graphene sheets rolled together bonded through weak Van der Waals bonds. This version of the CNT is called Multi Walled CNT (MWCNT). The diameter varies based on how many sheets that are rolled together but are typically in the range of 2-50 nm. If the anode contains metal catalyst such as iron or copper the Single Walled CNT (SWCNT) is produced in the form of soot. The two CNT structures are illustrated in Fig. 2.1. Producing SWCNT is delicate and costly due to high sensitivity and it is often difficult to get high purity content.

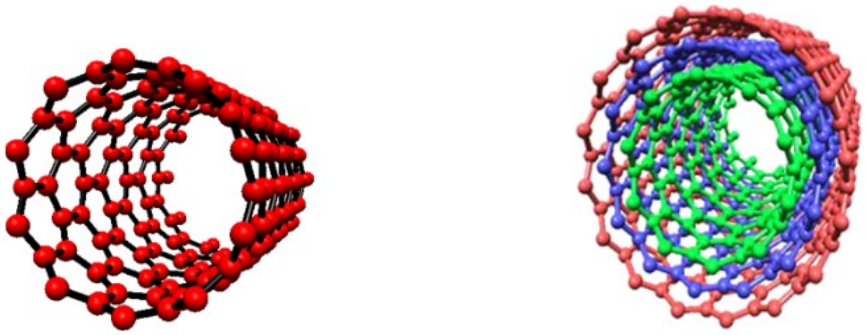

(a) SWCNT (b) MWCNT

Figure 2.1: Illustration of CNT structures gathered from [10]

2.1.1 Photo ignition of CNT

The ignition capabilities of CNT was first discovered by Ajayan et al. [1]. They discovered, by accident, the ignition potential of SWCNT when exposed to camera flash at close range. They found that the sample burns down in air, generating CO and CO_2 and leaving oxidized catalyst particles such as iron (Fe). Ajayan et al. explained this phenomenon by a heat pulse, absorbed in the CNT which could not efficiently dissipate due to the structure of the material. Ignition was only achieved on SWCNT that was dry and "fluffy", thus explaining the importance of the particles arrangements.

Braidy et al. [11] later confirmed this principle by reproducing the experiment with 23 wt% of Fe and found the formation of a bright, orange material by the end of the burning. They concluded that the process exceeded the melting temperature of Fe at 1538 °C since Fe_2O_3 with small amounts of Fe_3O_4 were found by X-ray diffraction analysis in the product. The following two stage reactions are explained by Sysoev et al. [12], where the first stage of heat release after PI is explained by either 2.2 or 2.1

$$3Fe(s) + 2O_2(g) \longrightarrow Fe_3O_4(s) \tag{2.1}$$

$$4Fe(s) + 3O_2(g) \longrightarrow 2Fe_2O_3(s) \tag{2.2}$$

Where s refers to the solid state and g the gasous state. The next stage is the heat release due to carbon reacting with oxygen.

$$C(s) + O_2(g) \longrightarrow CO_2(g) \tag{2.3}$$

$$C(s) + \frac{1}{2}O_2(g) \longrightarrow CO(g) \tag{2.4}$$

Smits et al. [13] found one year later that the PI of SWCNT is dependent on the Fe composition of the nanotubes. Purified samples were not subject to ignition, thus the flash ignition was attributed to the pyrophoric nature of fine Fe particles rather than any other properties in the SWCNT. The authors suggested that the SWCNT acts like a stabilizer for the Fe nanoparticles, allowing accumulation of thermal energy to reach the right temperature to oxidize before being released by a suitable energy source such as a camera flash. The work of Tseng et al. [14] discovered that both SWCNT and MWCNT are oxidized by flash because of the increase in the CO_2 concentration with the number of flashes on the samples. Tseng et al. also confirmed that the amount of catalyst play a key role in regards to the actual ignition and that a higher content of catalyst allows for easier ignition.

Chehroudi extended this idea in 2008 by measuring the minimum ignition energy on SWCNT samples utilizing a Xe based camera flash [15]. Chehroudi reported that the pulse width of the camera flash plays an important role in determining the minimum ignition energy as samples were easier to ignite when the pulse was kept short. Wavelength was found to be less significant than pulse width. The study reported that minimum ignition energy is a function of particle spacing as "fluffier" samples required less energy for ignition. The ignition process is more gradual and less well-defined in moderate and heavily compact samples, whereas the issue is drastically reduced in oxygen rich environments. Later on in 2018, Trewartha et al. performed a similar study, replacing the Xe flash with laser initiation to look at the behaviour of Fe content and output temperatures by utilizing a pyrometer [16]. This study found that maximum temperature increases with wavelength where 532 nm resulted in <1000 C° and 1064 nm were between 1000-1300 C°. It was found that 66% ferrocene by weight had the greatest output temperature and no significant effect were found between SWCNT and MWCNT.

2.1.2 CNT as an ignition agent

Although the thermal properties of the various types of CNTs have been thoroughly examined, the potential as an ignition agent for CVCC and motor applications are still immature. Cheroudi et al. were the first to accomplish PI on small droplets of various liquid hydrocarbons that are considered difficult to ignite and the author patented the idea for use in HCCI engines [17]. The experiment was conducted on a small glass plate with a mixture of SWCNTs and a few fuel droplets exposed to nearly atmospheric conditions. They noted that the fuel burns off much faster than the CNTs and that the flame itself would enhance the burning of the nano particles, leaving a much denser and harder product. An important finding in this study was that combustion only occurred if the CNTs were immersed in an overly oxygen-rich environment. Later on two more systematical studies were done by Cheroudi alone [15], [18]. He proved the concept as a distributed ignition method and allowing ignition to occur at multiple points. He argued the potential for PI to be utilized in both liquid fuel sprays and in a gasous mixture. In these studies an oxygen jet was directed towards the fuel/CNTs samples to ensure successful ignition.

To the best of this author's knowledge, only three papers regarding successful PI in a CVCC have been published. The studies have unambiguous results, proving PI more efficient than SI in a CVCC [2], [8], [9]. Methane, liquid petroleum gas, ethylene and hydrogen were subject to PI. Every fuel were greater than SI in terms of peak pressure, pressure gradient, ignition delay and fuel rate consumption for all tested fuel to air ratios. Studies performed by Carlcucci et al. utilized initial pressures of 6 bar and samples of 20 mg with Fe content ranging between 25-75 wt%. Berkowitz on the other hand managed to ignite an ethylene/air mixture with initial pressure at 1 bar, samples of 2 mg and Fe content of 70 wt%. What these studies had in common was the Xe based light located inside the CVCC allowing the flash to radially extend in the chamber. This method is not a sustainable alternative for the harsh environment inside a CVCC, nor a feasible alternative in an engine cylinder.

2.2 Combustion

Combustion is a high temperature exothermic reaction usually classified into three main phases. First is the ignition delay period which is the period from an ignition trigger, followed by a flame growth until the flame rapidly evolve. The next phase is often called the flame propagation phase where the pressure gradient reaches it maximum value and the majority of the fuel is consumed. The final phase is the after burning which occur after the peak pressure, this is characterised by a pressure decay as the heat leaves the system.

For a substance to combust and undergo a thermochemical reaction there has to be three elementary components present; an oxidant, a reductant (fuel) and a sufficiently high enough energy level to trigger the combustion. This energy level is referred to as the Minimum Ignition Energy (MIE) The substance prior and after combustion are named reactants and products respectively and the combustion characteristics as well as the product composition are highly sensitive to the composition of the reactants. The overall reaction is the balance between the reactants and the final product but consist of a large number of elementary reactions. These chemical mechanisms have complicated rate laws and are often very complex to describe [19]. Therefore, elementary reactions and product composition is outside the scope of this thesis.

2.2.1 Mixture compositions

There are multiple models to describe gas behaviour depending on the complexity of the gas composition and operating range in terms of thermodynamic states. Equation. 2.5 is chosen for this thesis and used through all pre-combustion applications.

$$\frac{n}{V} = \frac{p}{ZT\bar{R}} \tag{2.5}$$

Where p is the gas pressure, V is the volume, n is the mole amount, Z the compressibility factor, T the temperature and $\bar{R}$ the universal gas constant with the value 8.314 $[\mathrm{J}\cdot K^{-1} \cdot mol^{-1}]$. The mole amount is normalized by the volume because the volume in this thesis remains constant throughout. For simplicity, the compressibility factor is set to 1 because gas law applications in this thesis are far from the critical pressure and temperature of the gases involved, thereby assuming ideal gas behaviour. As for the mixture compositions, air-standard cycles are in most cases treated as ideal cycles even when the gas mixture consist of fuel. The percentage of fuel is often low, hence only a small deviation from the ideal gas assumption. [20]

Dalton's law of partial pressures for ideal gas mixtures states that the pressure of a mixture of gases is equal to the sum of the pressures each of its components (j) would exert if alone in the volume of the mixture at the same temperature. This can be described mathematically by Eq. 2.6

$$p = \sum_j p_j \tag{2.6}$$

Furthermore, the relative amount of a substance in a gas mixture is given as the molefraction (Y), whereas the sum over each substance corresponds to unity.

$$Y_j = \frac{n_j}{n_{tot}} = \frac{p_j}{p_{tot}} \tag{2.7}$$

To calculate the mixture compositions in a fuel/air mixture, stoichiometry is often utilized. Stoichiometry refers to a perfect relationship between reactants and products where all the reactants are consumed. For an arbitrary hydrocarbon consisting of only carbon and hydrogen (C_xH_y) the generic stoichiometric reaction equation in air is given by Eq. 2.8.

$$C_xH_y + z(O_2 + 3.76N_2) \longrightarrow xCO_2 + \frac{y}{2}H_2O + z3.76N_2 \tag{2.8}$$

Equation. 2.8 assumes only formation of CO_2 and H_2O as a results of the reaction and that nitrogen (N_2) does not take part in the combustion. Secondly, the air composition consist only of Oxygen (O_2) and N_2 at a ratio of 3.76, N_2 to O_2. The stoichiometric coefficient (z) is then found by balancing the reaction equation resulting in Eq. 2.9. For example, for CH4 the stoichiometric coefficient is 2.

$$z = x + \frac{y}{4} \tag{2.9}$$

Looking at the reactants, the fuel to air ratio (FAR) can be described by the partial pressures of fuel and air.

$$FAR = \frac{p_{C_xH_y}}{p_{O_2} + p_{N_2}} \tag{2.10}$$

Finally, an important parameter is the equivalence ratio (ϕ) which is defined as the actual fuel to air ratio relative to the stoichiometric fuel to air ratio (FAR_{st}).

$$\phi = \frac{FAR}{FAR_{st}} \tag{2.11}$$

In practical terms, the value of ϕ defines the fuel content in a mixture relative to the stoichiometric ratio. $\phi < 1$ corresponds to a lean fuel mixture, $\phi = 1$ is stoichiometric and $\phi > 1$ is a fuel rich mixture. Complete combustion occurs for lean and stoichiometric fuel composition, if fuel and air are well mixed and the criteria is that fuel completely reacts with the oxidizer. Moreover, a fuel has a flammability limit in terms of a range between different ϕ, where the fuel is able to combust. This range is dependent on many factors including pressure, temperature, ignition method and substance.

2.2.2 Constant volume combustion

A process in a CVCC is defined as an isochoric process which is a constant volume process, resulting in zero work output. These processes are ideal for combustion analysis as volumetric changes are excluded from the governing equations. Therefore, CVCC is often used to determine important combustion characteristics at varying inlet pressures, mixture compositions, temperatures and turbulence intensities to name a few.

Regarding combustion temperatures in a CVCC, the constant volume adiabatic flame temperature is a reference temperature as it shows the maximum temperature a combustion process can cause. It is defined as the resulting temperature of a complete constant volume combustion without heat transfer or change in kinetic and potential energy.

2.2.2.1 Ignition delay and the pressure gradient

The ignition delay (τ_d) is a good reference parameter in the first combustion phase and is defined as the time between the ignition trigger ($\tau_{trigger}$) and until the time where pressure has reached a certain percentage of the peak pressure. In this thesis 10% is used which is often used for SI. [21]

$$\tau_d = \tau_{0.1p_{max}} - \tau_{trigger} \tag{2.12}$$

As for the flame propagation phase, the time dependent pressure gradient is a measure on the combustion intensity. A large pressure gradient is the result of a rapid heat release and flame velocity. The heat release rate is proportional to the pressure gradient this could be shown by the idealized first law of thermodynamics for an isochoric process. [22]

$$\partial Q_{net} = \frac{1}{\gamma - 1} V dp + \delta Q_{ht} \tag{2.13}$$

Where Q_{net} is the heat release, Q_{ht} the heat loss, γ the specific heat ratio and V the volume of the vessel. The pressure gradient can be calculated from Eq. 2.14.

$$\frac{dp}{dt} = \frac{p_{n+1} - p_n}{t_{n+1} - t_n} \tag{2.14}$$

2.2.3 Spark ignition

SI is a single point ignition method found in for example Otto engines that utilize a high voltage electrical circuit to ignite a gas. The SI principle is an energy deposition into the gas by an electrical discharge between two electrodes, causing formation of plasma. As a shock wave is emitted during the expansion of the plasma a characteristic flow field is induced and ignition is initiated from a kernel. At this point the process experience rapid heat losses and the kernel has to grow beyond a critical size so that the flame sustain itself by heat release rather than be subject to extinction, also called quenching. Depending on the spark plug gap, which is the distance between the electrodes, the shape of the initial flame kernel is either nearly spherical or toroidal.

Combustion characteristics varies with many spark plug parameters such as the spark energy and spark plug gap. A recent study by Badawy et al. argues experimentally that the effect of spark plug gap is dominant for lean and stoichiometric mixtures, while rather insignificant for rich conditions [23]. The initial flame kernel radius was approximately the same for 1, 1.2 and 1.4 mm gaps, but the kernel growth is significantly larger for the latter. A visual interpretation for different equivalence ratios and gaps are shown in Fig. 2.2. Most importantly, the study showed that the pressure, flame speed, heat release and mass fraction burnt increases with the gap. Therefore, one should be careful when comparing other ignitions method to SI due to the sensitivity of the spark-plug type.

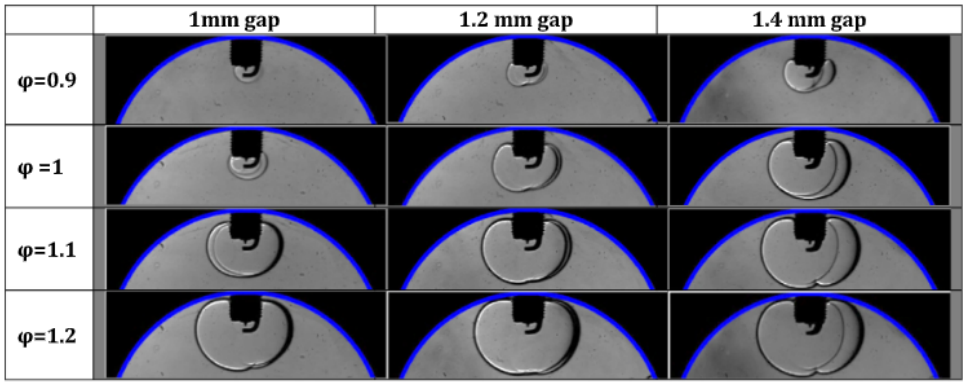

Figure 2.2: Kernel development after 6 ms from SI with variations in sparkplug gap and equivalence ratios gathered from [23]

2.2.4 Combustion of CH_4

CH_4 is a hydrocarbon consisting of one carbon and four hydrogen atoms. The fuel is viable in both the gaseous and liquid state, however in this study only the gaseous state of CH_4 are being tested.

The main reference studies used in this thesis are Reyes et al. comparative study on CH_4 and air mixtures looking at the effects of temperatures, pressures and mixture compositions, Cui et al. investigation on MIE and Huang et al. looking at the flammability limits at elevated pressures [24]–[26].

Figure 2.3 shows a typical pressure curve with varying initial pressures at stoichiometric conditions. The peak pressure between each curve is close to linear as the pressures moves from 0.05 to 0.15 MPa. Another important feature is that the ignition delay decreases with the initial pressure, while the combustion duration increases.. Regarding composition, a local maximum on the pressure is typically found around $\phi = 1.1$ for CH_4, which also yields the maximum flame speed. Furthermore, combustion peak pressure increases non-linearly with an increase in initial temperature and this correlation is most decisive at higher initial pressures and fuel rich mixtures while nearly identical for lean and stoichiometric. The study also showed that the peak pressure variation is much larger for lean mixtures than rich, where the difference is only moderate in the interval $1 \leq \phi \leq 1.2$.

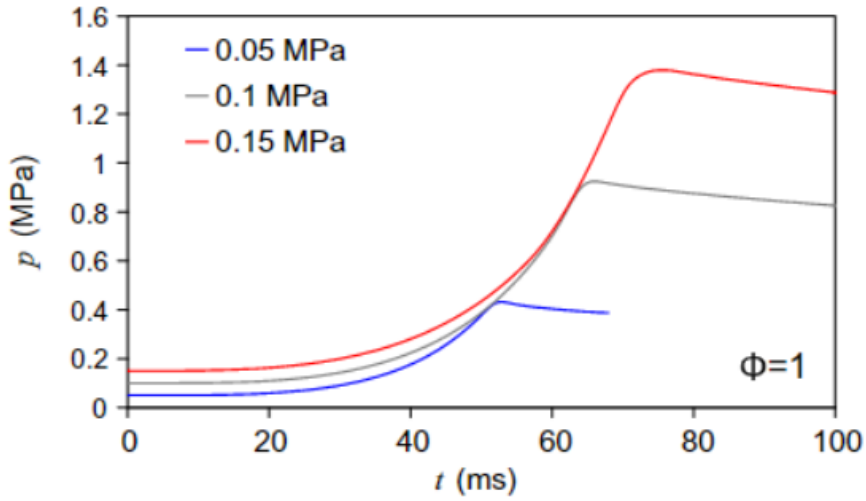

Figure 2.3: Pressure development of a stoichiometric CH_4/air mixture at different initial pressures. [24]

The MIE of CH_4 depends on many things such as pressures, temperatures, substance and composition, but also ignition specifics. For instance, in SI the MIE is sensitive to the spark plug gap, storage capacitor and storage voltage, according to Cui et al. Therefore, in their study they kept the gap at 1 mm while measuring voltage and current during the spark duration to keep these constant. Figure 2.4 shows the relation between the MIE and ϕ in 2.4a and the MIE, pressure and temperature relation in 2.4b. At fixed pressure, temperature and spark plug gap the MIE has a local minimum at stoichiometric mixture composition. Variations are also greater

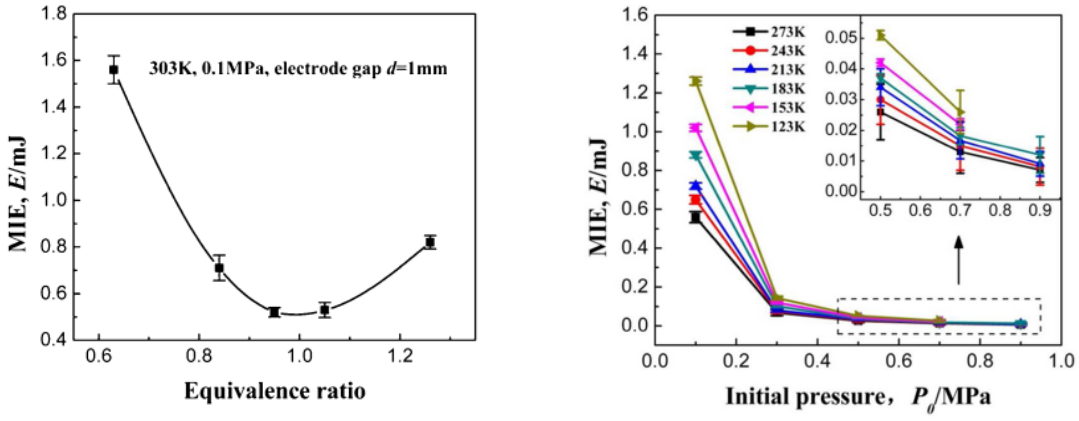

(a) MIE as a function of ϕ

(b) MIE as a function of p and T

Figure 2.4: MIE of CH_4 from [25], the left figure shows the variation with ϕ and the right figure shows the pressure dependence at a set of constant temperatures

for lean than that of rich mixtures which implies that rich mixtures are easier to ignite than lean. It should be noted that with SI there has to be enough fuel between the electrodes for a kernel to grow, which is why it is not uncommon to add fuel in the vicinity of the gap when burning lean.

For the pressure and temperature variations, the MIE drops with an increase in both. However, the MIE is proportional to $1/p^2$ while only $1/T$, where the subscript naught denotes the initial conditions just before ignition. It is shown from 2.4b that at low initial pressures, the temperature greatly affects the MIE and as the pressure approaches 3 bar the MIE start to converge and the temperature variations becomes less significant. The same goes for low initial temperatures, where pressure greatly affects the MIE, whereas the effect of pressure is less significant when the temperature is kept high.

Finally, the flammability limit for standard atmospheric condition of CH_4 ranges from $\phi = 0.5$ to 1.7 [27]. However, an increase in initial pressure increase the upper limit and slightly decrease the lower limit. The study also show that the maximum combustion pressure varies linearly with the initial pressure for mixtures around the lower limit, while there are greater deviations for this relation on the upper limit [26].

2.2.5 Flame characterisation

The aim for the flame in the CVCC is a premixed flame with low turbulence. To determine that goal it is important to distinguish between different types of flames. In general there are two main types of flame being premixed and non-premixed. Furthermore, because of the effects of turbulence on the combustion process the two categories are often defined by the turbulence intensity of the flow field, pre combustion. Turbulence enhances mixing, increases burning velocities, accelerating the heat production and the pressure rise [28]. Moreover, a full analysis on the

turbulence description of the flames was outside the scope of this thesis.

2.2.5.1 Non-premixed flames

A non-premixed flame, also called a diffusion flame has variations in the local equivalence ratios and can in theory cover the whole range from $\phi = 0$ (air only) to $\phi = \infty$ (fuel only). Rich and lean combustion occur at the same time with a less localized flame front that tends towards stoichiometric condition, $\phi = 1$. [19] Due to the variations in equivalence ratio the combustion tends to be slower. Every locally fuel rich point in a carbon-based mixture produce more soot because of the lack of oxidizer. The soot typically becomes incandescent from the heat of the flame, attributing the flame an orange color with black smoke.

2.2.5.2 Premixed flames

Premixed flames on the other hand have fuel and oxidizer available throughout the entire mixture since the equivalence ratio is homogeneous. Once the combustion is initiated the combustion process sustain itself by its own heat release until the entire charge is fully depleted. Due to the uniform charge, the combustion occur with much greater control than that of a diffusion flame. Premixing allows for leaner mixtures leading to lower temperatures and therefore lower production of nitric oxides (NO). However, a premixed charge can lead to spontaneous ignition if the MIE is reached by for example an increase in pressure or temperature. Premixed flames tends to have a characteristic blue color when burnt complete since soot are not formed. However, in fuel rich combustion the flame can have an orange outer diffusion flame because of the formation and burning of CO. [29]

Chapter 3

Methodology

In this chapter the methodology of various tasks towards the main goal of achieving successful PI is explained. First off, the flame analyzed in previous work was characterised as non-premixed due to the lack of a gas mixing device. Therefore, a developed gas mixing device and the method to determine the gas mixing procedure were proposed as well as strategies to validate the mixtures homogeneity.

As stated in 1.3 the CVCC had mixed results with large deviations at the same initial conditions. A major objective for this thesis was therefore to control and confirm the mixture composition. Moreover, the method for which a complete combustion analysis with SI, targeting a premixed low turbulent flame, was investigated with the purpose of validating the CVCC and having a comparative case between SI and PI.

Afterwards, the CNT injection strategies were looked at and established through a high speed camera set-up to determine flash timings and CNTs dispersion in the chamber. Finally, three different strategies for attempting PI of the CNTs with an externally mounted Xe based light source was proposed. Different configurations were looked at in detail to map out the limits and the potential for PI.

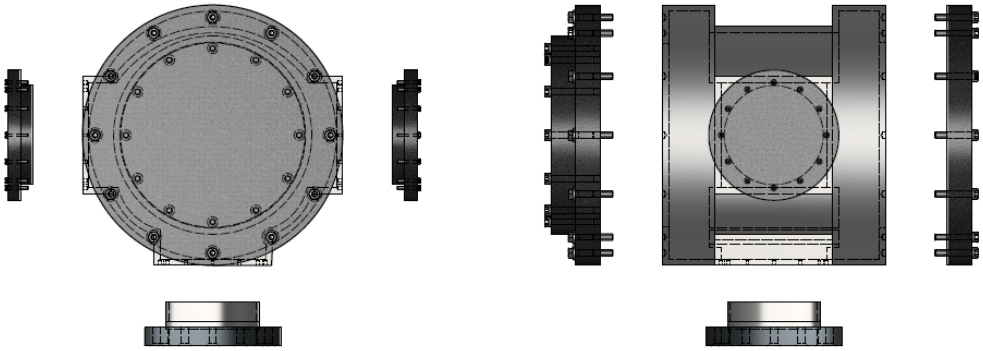

Figure 3.1: Front and side view of the CVCC and the different components

3.1 Experimental setup

A graphical illustration of the cylindrical CVCC is shown in Fig. 3.1. The main chassis is made out of stainless steel and have five different openings with five different lids made out of cast iron. The large lids are where the injection of the different gases are mounted as well as the measuring tools which include a manometer and a thermocouple. The smaller lids are there to hold the spark-plug and the quartz glasses for optical access in place. The lid placed underneath the chamber is for a gas mixing fan device. All lids are equipped with inner seals to avoid gas leakage, while the quartz glass module have two seals for protection of metal to glass contact.

The gases involved in the procedures were primarily synair with a fixed composition of 79 % N_2 and 21 % O_2, CH_4 and pure N_2. Synair and CH_4 were supplied from a central gas system, while N_2 was supplied from a bottle. These were all equipped with a regulating valve to set the pressure and magnetic solenoid valves for controlling the gases by a `labView` software. All gases were filled sequentially with compositions determined by partial pressures.

For the general experimental setup, Fig. 3.2 illustrate the P&ID. It should be noted that the configuration was such that the fuel and air was directly injected into the CVCC without any mixing, hence the gas mixing procedure occured inside the chamber. The software took the initial air pressure (p_a) and the target equivalence ratio (ϕ_T) as input parameters and as the filling took place the pressure transducer (P1) measured the chamber pressure. The solenoid valve then closed as the target air pressure was reached. As fuel was injected, the control-program continuously solved Eq. 2.5 for the amount of moles based on the instantaneous pressure and the temperature. To determine the right amount of CH_4 the criteria for the final pressure is stated in Eq. 3.1, which is just a combination of Eq. 2.10, 2.11 and 2.6. The solenoid closed as this pressure was reached.

$$p_{CH_4} = p_{tot} - p_a \longrightarrow p_{tot} = \phi_T \cdot FAR_{st} \cdot p_a + p_a \tag{3.1}$$

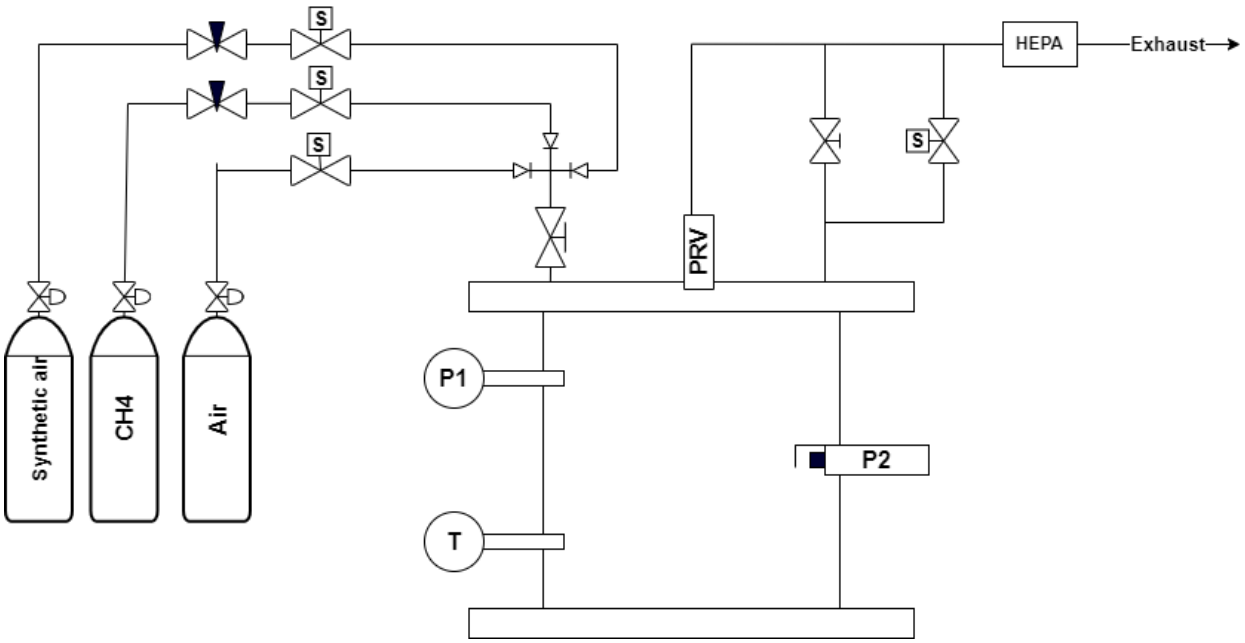

Figure 3.2: Process and instrument diagram for a combustion bomb with SI of CH_4/air mixtures, P1, P2 and T represent the sensors. Solenoid valves are denoted with **S**

Without any further procedure the mixture is then categorised as non-premixed and the only gas mixing that occured inside the chamber was due to the axial velocity of the injection jet and a minor mixing by pressure. As the mixture was ready to combust, a signal was sent to the spark-plug with a set delay and the piezo electric pressure transducer (P2) was activated as the combustion took place, logging the data at a frequency of 10 000 Hz. After the combustion, the exhaust gases were released through either a solenoid valve, manual valve and in worst case a Pressure Relief Valve (PRV) with a set pressure of 41.5 bar. The gas escaped the system through a High Efficiency Particulate Air (HEPA) filter.

The spark-plug was a `Bosch` FR7KPP332 Platinum spark-plug with a constant gap at 1 mm. P2 was mounted on the spark-plug which is fitted through a metal plate and sealed by the smaller lids to the chamber. The entire experimental setup is shown in Appendix A.

3.2 Pre-Combustion procedure

As mentioned in section 1.2, an important aspect before attempting PI of CNT's was to verify that the CVCC was functioning in a reliable and trustworthy manner. Therefore, the purpose of this section was to set the frame for a base study to get the CVCC to deliver similar results to that of the reference studies discussed in section 2.2.4. This primarily involved getting the real equivalence ratio ϕ as close to the targeted equivalence ratio ϕ_T as possible.

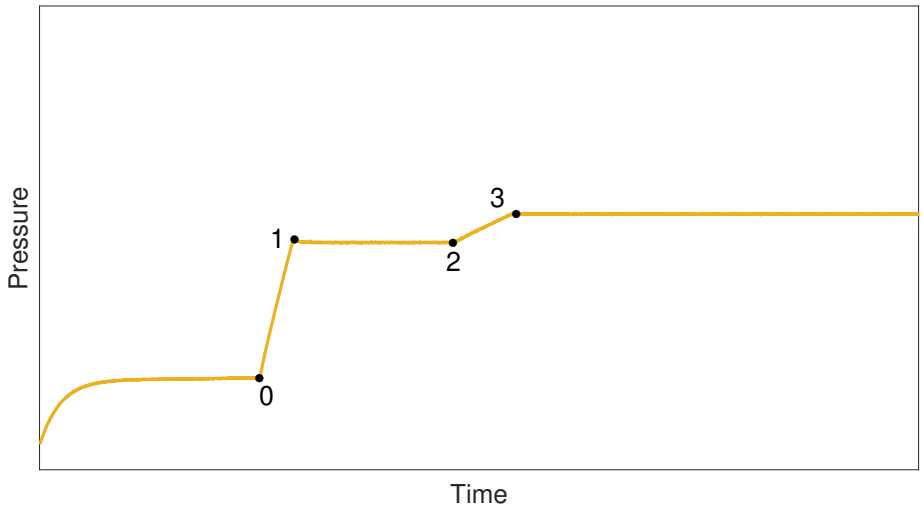

Figure 3.3: Pressure development in time during the gas filling procedure. State 0 to 3 represent the time between the start of air filling and until the target composition is reached

Figure 3.3 shows the pressure variations with time as gas filling occurred. Each of the states have a corresponding temperature value and the mixture composition was determined from the states and calculated by the equations presented in 2.2.1. Air filling occurred from state 0 and up until state 1 with the pressure and temperature, p_a and T_a at 1. Between state 1 and prior to fuel filling at state 2 there was a delay (t_{1-2}) to stabilize the pressure and temperature before filling fuel up to state 3. At state 3, the mixture composition was set followed by another delay. This delay was created so that the gases had time to mix and turbulence to dissipate. Combustion occurred at the end of that delay with the pressure and temperature denoted as p_t and T_t. At these reference values the combustion trigger was activated. For SI, 3 consecutive attempts without success classified the mixture as non-ignitable.

The exhaust system that rids the chamber of the end gases left the pressure at atmospheric pressure, meaning that after each combustion there was approximately 1 bar of burnt gases in the chamber. Therefore, it was of utmost importance to flush the system with synthetic air to ensure that the local atmosphere consist of synair alone. Flushing occurred from the start of the experiment and up until state 0. The flush time was experimentally investigated, and it was determined that 90 seconds was sufficient to rid the chamber of burnt gases. It should be noted that from this point and through the entire thesis, every single pressure referred to with

regard to the chamber is the gauge pressure. For example test at $p_a = 1$ bar yields the absolute air pressure at 2 bar.

Regarding t_{0-1} and t_{2-3}, two nozzle valves from Fig. 3.2 were installed to choke the flow and limit the pressure difference over the solenoid valves. This resulted in a slower filling procedure dragging out process 0-1 and 2-3. The reason for this was that the response for the solenoid valves to close was long, resulting in an overfilling of especially fuel into the chamber. Another important aspect of including these valves in the P&ID was to ensure synchronisation between the sensors. The thermocouple has slower response than the pressure transducer, so the target was to get the processes as isothermal as possible.

After standardizing a pre-combustion procedure and verifying the mixture composition and its homogeneity, the test matrix with p_a from 1 to 4 and ϕ_T from 0.6 to 1.30 was aimed for. The range of ϕ_T was extended from the determined flammability limit in section 1.3 to compare if the new procedure had any effects on the flammability limit. Finally, the reference temperature T_t was targeted to 25°C.

3.3 Mixing fan

Several mixing strategies have been looked at, but it was decided to go for a fan-based solution. A mounted electrical fan was out of the question due to the complexity of this configuration. It was therefore decided that a fan driven by a magnetic stirrer was the easiest accessible solution. The stirrer was a type `VELP Scientifica` F20320164, primarily used for stirring liquids in chemical applications. The stirrer had 10 different modes ranging linearly from 0 to 1200 rpm.

Since the fan would operate in a harsh combustion environment, frictional forces were the main concern. Combustion produces soot and water vapor amongst other substances, which would increase the friction between the surfaces. The magnet was also driven by an external source, where the magnetic field strength is inversely related to the distance away from the source. Therefore, it was critical to get the stirrer as close to the chamber as possible. A platform for the magnetic stirrer to be able to adjust its position along the 3 different axis was assembled by `THORLABS` equipment. The assembly ensured that the stirrer was placed as close to the magnet as possible as well as providing a tool for fine tuning along the width and depth. The finalised setup is shown in Fig. 3.4.

As for the fan geometry, a swirl-based and a lift-based design were created by 3D-modelling before 3D-printing and afterwards the model was tested in the chamber. As a complete study on the flow-field created by the fans was outside the scope of this thesis, the designs were instead evaluated in terms of stability and consistency ranging at all speed levels. For the base of the fan, it was important to design it in a way so it would self-recover if forced out of position. Also, it was important to manufacture the fan in metal so that it could withstand cycles of high temperature exposure. Aluminium was chosen because of its non magnetic properties and low weight.

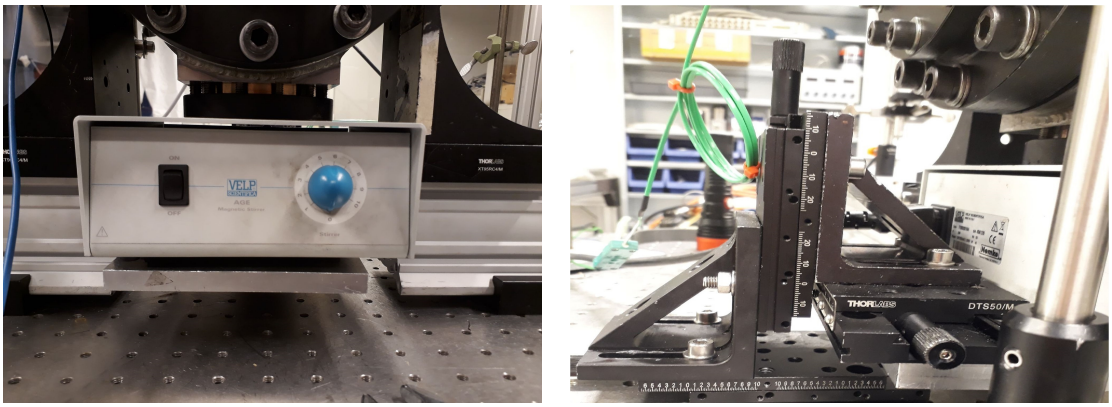

Figure 3.4: Finalized mixing module with magnetic stirrer and a 3-axis tuning assembly

The finalized design was a drag-based fan, with a rectangular base for the magnet to fit into. The module is illustrated in Fig. 3.5. The flaps were first meant to be curved to push the gas upwards as well as create a swirling motion, but this was later neglected to make for easy manufacturing. The fan was made out of an aluminium U-profile with two plates welded on each side at the center. The magnet was then glued with temperature resistant glue inside the U-profile and the magnet to metal contact surface was coated with a thin layer of oil to reduce friction.

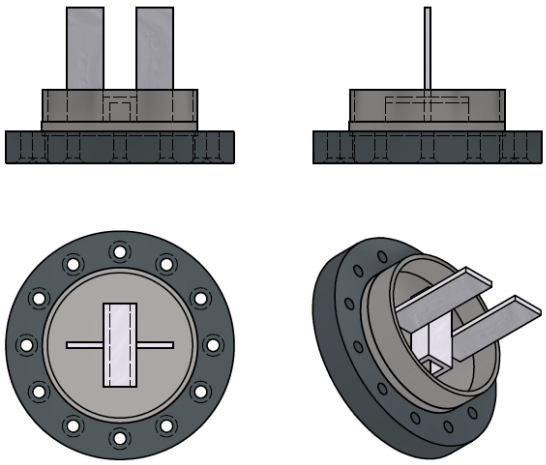

Figure 3.5: Fan module, consisting of the outer lid, the inner ring and a swirl based fan geometry. Magnet fits inside the rectangular base

To verify that the fan configuration indeed gave a premixed low-turbulent flame, two methods were utilized. First, the homogeneity of the mixtures composition was examined by looking at the consistency of the data for different mixing times (t_{mix}). t_{mix} is defined as the time from after gas injection where the total amount of moles are mixed together. Then, film the flames were filmed with a `Promon U750` camera for different times to visually observe how the flame develop. As for the turbulence intensity created by the swirl, different rotational speeds were subject for testing, primarily from 720 to 1200 rpm while holding t_{mix} constant. To target the low

turbulence flame a new time was defined (t_{ds}). This time is defined as the interval after t_{mix}, where the fan is turned off for the turbulence to dissipate. Different times were to be tested and the length of the interval was decided to be determined based on where the combustion pressure converged.

3.4 CNT Injection Strategy

Before getting to the CNT injection strategy, safety measures had to be made. As reported in [30], CNT poses a hazardous health effect, particularly for dry samples. Inhaling the particles can cause damage to respiration and lead to cancer. Therefore, in accordance to the HSE procedure, handling of CNT were confined in a seal glove box. If samples were carried out, extensive protective gear had to be wore such as HEPA masks, glasses, protective suits and double layer plastic gloves.

For the injection, it was decided to transport the particles in a confined module with compressed gas, at a set pressure difference (Δp) between the injection line and the chamber. Multiple considerations had to be accounted for, factors such as pipe geometry, velocities and pressures, distances, particle amount, Fe-content and timings were all important aspects towards the ultimate goal of successful PI of an combustible mixture. From section 2.1.1, it is favorable for the particles to have such spacing that they are dense, but not to the point where oxygen is not allowed to partake in the reactions. Regarding the composition, based on Trewartha et al. study on output temperatures by PI of CNTs, 66 wt% Fe would be used as the main composition as this yields the largest temperature output.

The original thought was to create 3 different outlet pipes, one reducer, one regular and one expander to see the effects on the CNTs distribution around the quartz glass. Due to the lack of suitable reducers only the expander and the regular were made and tested. Moreover, the injection strategy was then determined by testing three different amounts of particles and Δp.

3.4.1 CNT injection line

The developed injection P&ID is shown in Fig. 3.6, where the CNTs leave the pipe in the chamber and was injected towards the quartz glass. The pipes have an outer diameter of 6 mm and a wall thickness of 2 mm. All fittings and valves, except the solenoid, are from `Swagelok` and every male to female connection is equipped with an inner and outer ferrule. The chamber connection named **BT** was a 6 mm bored-through fitting and inside the chamber was an attached variable pipe bend to direct the particles towards the quartz glass. The injection line was set up so that the injection gas can vary between N_2 and synair. Several different placements of the solenoid was tested but it was determined that the placement had to be prior to the CNT capsule to avoid clogging. A one way valve was mounted between **BT** and **CNT**, but had to be removed for the same reason. Therefore, the extra manual valve was installed instead to shut of the CVCC from the CNT circuit.

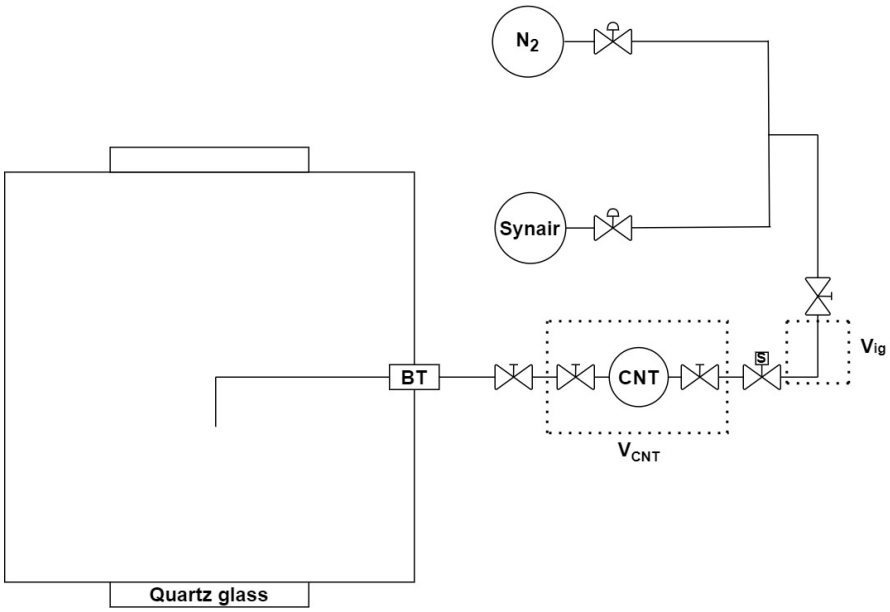

Figure 3.6: Process and instrument diagram for CNT injection based on N_2 or synair gas flow

There are two confined volumes of importance in this diagram, being V_{CNT} and V_{ig}. V_{CNT} was the volume that the CNTs module holds and it consist of a T cross fitting for filling CNTs, and two manual valves to seal the volume off due to the hazardous effects. The module is taken off the P&ID and into a sealed glove box while adding CNTs. V_{ig} is a fixed volume with the purpose to control the amount of gas being injected in the chamber at each injection test. It was confined by a solenoid valve that controls the injection and a manual valve to seal of a fixed amount of gas. Therefore, the amount of gas in V_{ig} was only determined by pressure and gas type. Lastly, the solenoid valved was programmed in such a way that it activated either a camera flash or a high speed camera with a set delay (t_f), after activating the valve. t_f was the parameter that was subject to investigation to determine exactly when to activate the flash after injection of CNTs.

3.4.2 Optimal flash trigger

To determine reasonable values for t_f a high speed camera rig was set up as illustrated in Fig. 3.7. The camera was a Photron Fastcam NOVA S6 able to film with a frame speed up to 6400 frames per second (fps), while maintaining a resolution of 1024x1024. As for this setup the spark-plug was replaced by another quartz glass to get continuous lightning through the chamber. To ensure an uniform distribution of light, a diffuser was mounted close to the quartz glass with a light source at a set distance from it. All components were mounted on railings such that their position can vary to optimize the quality of the pictures.

After filming an injection the raw images were processed through a `MATLAB` script, shown in Appendix C.1. The script looped through all the frames in the respective injection test while calculating the grayscale of each pixel in the 1024x1024 resol-

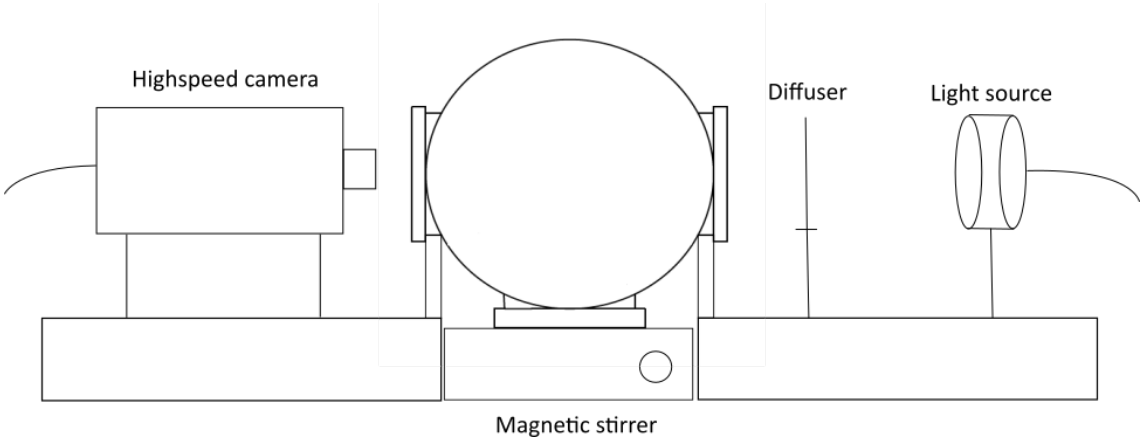

Figure 3.7: Experimental setup to determine t_f through image processing with a highspeed camera

ution. Seeing that the CNTs were black particles the program calculated the level of darkness for each picture and gave out the darkest picture, in other words the picture with most dense particle distribution. Based on the frame position and the fps, t_f was determined so that the PI was activated at the best possible time with regards to the particle density distribution.

3.5 PI of CNT

The configuration for PI of CNT was very similar to that of the injection strategy method, only that the high speed camera was replaced by a `Godox AD600BM` camera flash. The camera flash delivered a maximum energy of 600 J at a flash duration of 4.5 ms. A complete study of the capabilities of the camera flash and the MIE for different samples was performed by Stian Ranøyen Bratsberg [31]. He found that the flash was able to ignite samples at a maximum distance of 5 cm. Since the quartz glass has a thickness of 3 cm, particles from the end of the quartz glass and 2 cm into the chamber should be able to ignite. Moreover, the flash delivered very high luminous energy. Therefore, to avoid damaging the fast camera the `Photron` was replaced by a `Promon U750` where a 800 fps with a 800x600 resolution was utilized.

Three main methods were utilized to attempt PI og CNT's. The three configurations were defined by the particle placing in the chamber and is summarized as:

1. ***Static CNTs placement*** was the method where particles were placed in the chamber and then exposed to the flash while remaining static. The two configurations for this method can be seen by the glass shelf and the basket in Fig. 3.8.

2. ***Dispersion***, was the method where particles were first placed in the chamber on the glass shelf and slightly before the flash trigger exposed to a gas jet leaving the pipe. Consequently, the particles were dispersed in front of the quarts glass just before the trigger, resulting in a particle distribution as close as possible to the window.

3. ***Injection*** was the injection method that was the developed from the CNT injection strategy section 3.4 with the optimal trigger time found later on in the CNT injection results 4.3.

As this was an investigative type of experiment without references articles, the majority of experiments were to be conducted one or two times. As the MIE of a flammable mixture varies quadratically with the pressure, the investigation started at the highest possible pressure. ϕ_T started at 1 which yielded the MIE. In addition, mainly three different CNTs amount (m_{CNT}) were to be tested; 12, 24 and 36 mg with a Fe content of 66 wt%. For simplicity, samples with other CNT/Fe ratios would still be characterised at these masses. This was done because the particles were handled by volume, see Appendix B.1 for more information. At these reference values the PI experimens were initiated, workout outwards to investigate the limits of this ignition method.

Figure 3.8: Illustration of particle placement setup. The three configurations were either static in the basket, on the glass shelf or injected through the pipe

3.6 Data analysis

The data was gathered from the thermocouple and the pressure transducers from the start to the end of a combustion experiment. The sensors converted the temperature and the pressure to a voltage signal through proportionality. Since the thermocouple was operating at a low frequency, it would not properly capture the temperature development during combustion and was therefore excluded from analysis. As for the high speed pressure curve, the piezo electric pressure transducer was activated 2 seconds before ignition trigger and logs 5 seconds after. The high frequency logging was therefore set on a 7 seconds period.

The raw data was logged in a Technical Data Management Streaming (TDMS) file and then processed through the `MATLAB` script seen in Appendix C.2. The script looped through a folder containing k number of files, formatting the time and filtering the data before calculating and storing the variables. For the ignition delay, the parameter was estimated by moving backwards in time from the end of the array, beyond the peak pressure and then find the value that corresponds to 10% of the peak pressure. The ignition delay period was simply this time minus the ignition trigger time. Finally, the data was plotted and cross examined manually by calculating the mixture composition by the theory presented in the mixture theory section (2.2.1).

The data is presented in the terms of the two statistics, the mean ($\overline{x}$) and the Sample Standard Deviation (SSD). Because combustion is stochastic by nature, all parameters with same inlet conditions was averaged before looking at the variations through the SSD of that respective parameter. The mean was given by Eq. 3.2.

$$\overline{x} = \frac{\sum_{i=1}^{n} x_i}{N} \tag{3.2}$$

Where x_i is the ith sample and N the sample size. Moreover, the SSD was calculated from the sample by Eq. 3.3.

$$SSD = \sqrt{\frac{\sum_{i=1}^{N}(x_i - \overline{x})^2}{N-1}} \tag{3.3}$$

As the experiments contains random and systematical error, the discussion and efforts to characterise these are listen in Appendix B.

Chapter 4

Results

In this chapter the results from the different aspects of the method are presented. As the fan configuration had to be in place before the combustion studies, the first results show the fan performance and how it defined the combustion procedure. Secondly, a combustion study of SI is presented at varying pressures and varying ϕ. The mixture composition as well as the combustion parameters are presented after being processed by the data analysis method explained in section 3.6. Finally, the results from looking at injection strategies to determine the flash trigger time are presented, followed by a study on PI.

4.1 Fan performance

The investigation of effects created by the fan was conducted by the method explained in 3.3 and the results are presented in this section.

As mentioned, the addition of a swirl-fan was expected to have an effect on both the turbulence intensity and the homogeneity of the gas. Therefore, the required time the fan had to be turned on before triggering the combustion was mapped out starting from 0 s (only during fuel filling) and up until 120 s with a rotational speed of 960 rpm. 120 s was the upper limit that was tested because it was found, by visual interpretation, that this was sufficient for the gas to be at an acceptable homogeneous state. A comparison between t_{mix} at 60 and 120 s is shown in Fig. 4.1 at time instances at 30 s and the end gases at 190 s. The mixture had local fuel rich points for t_{mix} = 60 s, while homogeneous for t_{mix} = 120 s. The differences between the mixing times could also be seen from the exhaust gases shown after 190 ms in Fig 4.8b and 4.1d. The shorter mixing time had local burning residues in the end gas and was in general more polluted than the longer mixing time, indicating a more incomplete combustion.

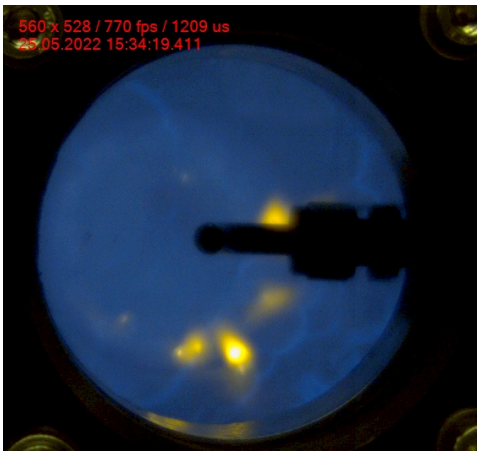

(a) t = 30 ms, t_{mix} = 60 s

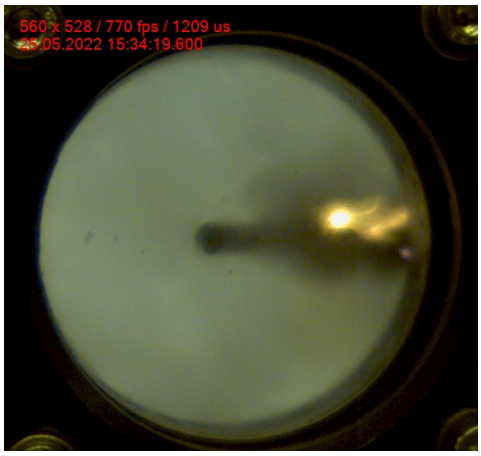

(b) t = 190 ms, t_{mix} = 60 s

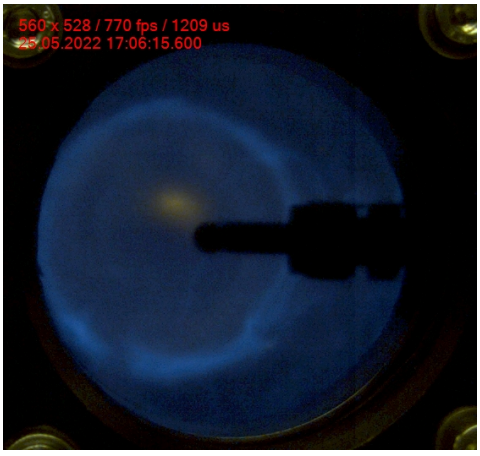

(c) t = 30 ms, t_{mix} = 120 s

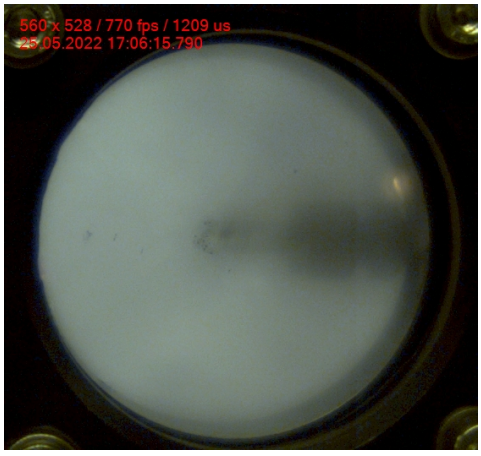

(d) t = 190 ms, t_{mix} = 120 s

Figure 4.1: Visual effects on mixing time for flame development and the burnt gases for SI at p_a = 1 bar, ϕ = 1.0 and fan rotational speed of 960 rpm

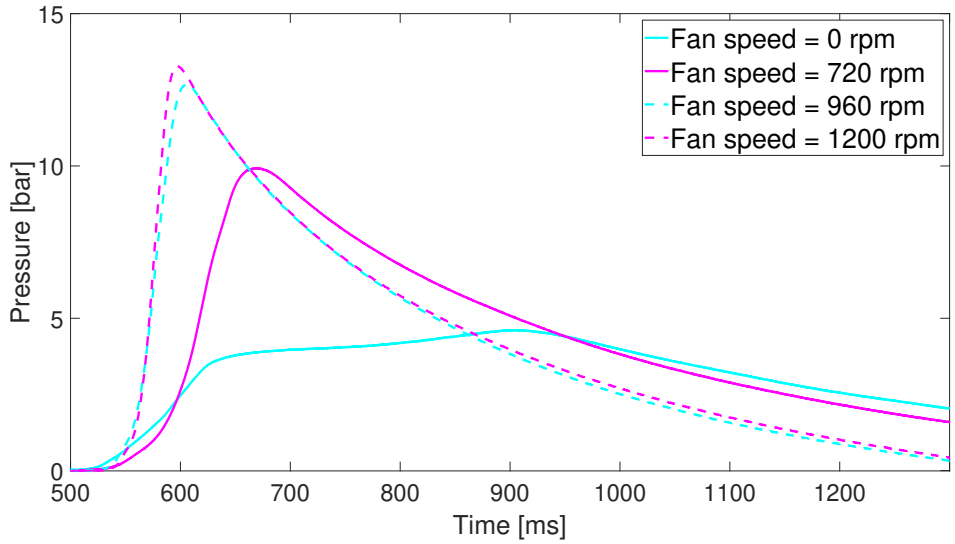

Figure 4.2: Combustion pressure curves from SI for different rpm at $\phi = 1$ and $p_a = 1$ bar. Ignition initiated while fan was on

After determining the t_{mix}, the effect from varying the rotational speed of the fan was characterized. The combustion pressure curve was utilized to look at the pressure development for 0, 720, 960 and 1200 rpm at $\phi = 1.0$ and $p_a = 1$ bar. Results are listed in Fig. 4.2.

The 0 rpm case was a reference case that shows the combustion without any fan, which means that the mixture was neither turbulent nor premixed. This case was limited by a low pressure gradient and a low peak pressure. Compared to the largest rpm at 1200, the case with 720 rpm had both a longer ignition delay and a smaller peak pressure. This could be a combination between incomplete mixing, since the mixing time was verified at 960 rpm, and a lower turbulence intensity. Finally, the curves for 960 and 1200 rpm were nearly identical. This could have been because the mixture was premixed for both instances and the effects between the two swirls at those rpm were negligible.

Since turbulence is hard to measure directly, the last experiment for the fan performance was to get an indication of how turbulent the flame was with fan speed at 960 rpm and $t_{mix} = 120$ s. The goal was to find a minimum time (t_{hold}) after the fan was shut off until the turbulence had dissipated to a state where it did not affect the combustion parameters. Figure 4.3 shows the development of the peak pressure as a function of t_{hold}, again at $\phi = 1$ and $p_a = 1$ bar. After about 150 s the peak pressure trended towards convergence and the effects from the first 120 seconds were relatively high with a maximum pressure difference of approximately 0.8 bar. As a result, t_{hold} was set to 150 s for the remaining experiments. As a final remark; varying p_a and ϕ could have had an effect on all the determined parameters. The time constraint limited both the amount of samples for the discussed cases and also the limits. $p_a = 1$ and $\phi = 1$ was chosen because of the target study by Berkowitz et al. [2]. The fan speed of 960 rpm, $t_{mix} = 120$ s and $t_{hold} = 150$ s were all kept constant for the rest of the experiments in this thesis.

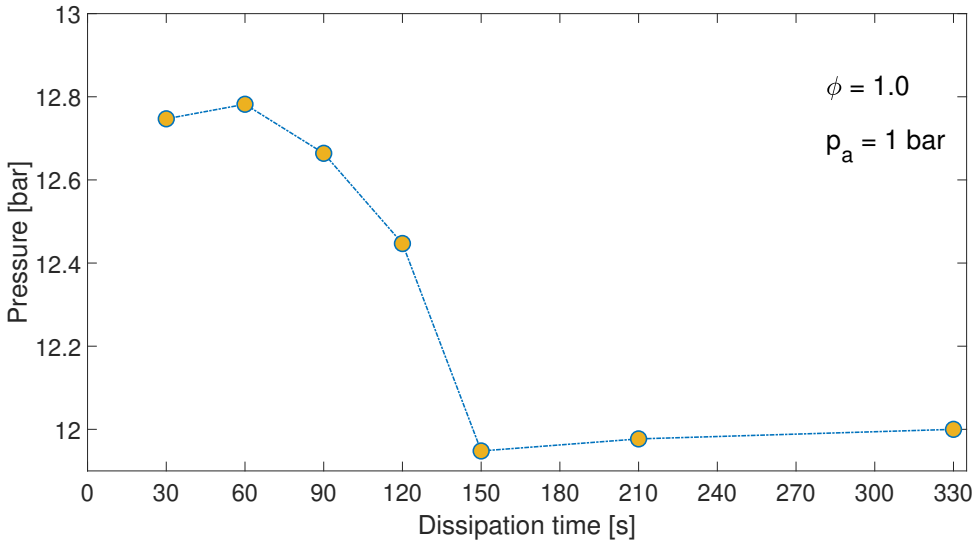

Figure 4.3: Peak combustion pressure variation with dissipation time from when fan is shut off after 120 second mixing time at $\phi = 1$, $p_a = 1$ and fan speed = 960 rpm

It was evident from the results that the fan was able to delivering a homogeneous mixture after the set time interval. Because of the method to determine the turbulence dissipation time it could not be said for certain that turbulence had fully dissipated at this time. This was only meant as an effort to reduce the effects of turbulence. Optimally, turbulence should have been visually observed through filming with the high speed camera, but was not prioritized because of the time constraint of the project.

The test regarding the mixing and dissipation times were conducted at the lowest tested pressure used in this project. Ideally, filming of combustion should have been conducted for a broader range of pressures and ϕ to ensure that the whole range of tested parameters yield the premixed, low turbulent assumption. For multiple reasons, it was later on decided to do a combustion time lapse at the highest tested pressure at $p_a = 4$ bar and at $\phi = 0.8$. By visual interpretation, the flame looked premixed and the combustion developed as expected for those initial conditions. This time lapse can be seen in later on in Fig. 4.7.

As for the for the performance in terms of reliability, the design came out to be reliable for SI but unreliable for PI. Since the module was placed at the bottom of the chamber, soot and impurities gathered on the surface. This led to an increase in the friction between the magnet and the metal. This was not an issue for SI, where only a simple cleaning procedure and a thin coat of lubrication was necessary after multiple days of combustion. For the injection tests, and ultimately the PI, the fan functioned in a particularly unreliable way. The gathering of vast amounts of CNTs combined with condensation from combustion led to the fan operating in a highly viscous environment. To ensure reliable results, extensive cleaning had to be done regularly, which was very time consuming, following the HSE procedure for CNTs handling. Operating in a high particulate matter environment, such as this, would required a pivoted fan driven by an external motor.

4.2 Spark-plug ignition

The experimentally determined standardized combustion procedure can be summarized with a flushing time of 90 seconds, a hold time after air filling and prior to fuel filling on 90 seconds, a mixing time of 120 seconds and a dissipation time of 150 seconds. The needle valves were adjusted for each pressures to the point where they spent the longest amount of time to fill the gases, but not so much that they did not reach the target pressure. Depending on the pressure, a typical combustion procedure took about 400-600 seconds with an approximate 20-30 minutes cool-down period after each successful combustion.

With the new standardized procedure, a combustion study on the CVCC performance and reliability were performed. A series of 120 different SI combustions was included and analyzed by the theory explained in the combustion section 2.2 and processed through the data analysis method in 3.6. Experiments were, as mentioned, performed in the range of p_a from 1 to 4 bar and ϕ from the flammability limit discussed in the combustion of CH_4 section (2.2.4).

Approximately half of all SI combustions were done at $p_a = 1$ bar to get a solid foundation of SI data at this pressure to compare with PI from Berkowitz et al. reference study. Table. 4.1 summarizes the correlation between ϕ and the combustion parameters at $p_a = 1$ bar. The values are represented by the means of the respective combustions with the SSD in parenthesis. As for the temperature at the trigger, the target was 25 °C, where the mean across all combustions was 25.81 °C with approximately 1.5 °C in SSD. The target pressure just before combustion was 1.20 bar, which was obtained by slightly varying p_a for each ϕ. The mean across all p_t came out to be 1.19 bar with a SSD at 0.02 bar.

As for the real ϕ, the measures discussed in section 3.2 seem to have had good effect. The target ϕ_T and the actual ϕ are close to each other in value, but with a slightly richer composition for all tested ϕ_T. The lowest deviation are at $\phi = 1.0$ with 1% while largest at $\phi = 1.1$ at 3%.

ϕ_T	T_t [°C]	p_t [bar]	ϕ	dp_{max} [bar/ms]	Ignition delay [ms]	p_{peak}
0.8	26.90 (3.80)	1.17 (0.02)	0.82 (0.02)	0.10 (0.02)	452 (241)	10.45 (1.52)
0.9	26.41 (1.13)	1.16 (0.03)	0.92 (0.02)	0.12 (0.01)	420 (215)	11.99 (0.89)
1	25.06 (0.13)	1.19 (0.01)	1.01 (0.01)	0.13 (0.01)	341 (83)	12.74 (0.24)
1.1	24.42 (1.81)	1.20 (0.01)	1.12 (0.03)	0.14 (0.01)	300 (114)	13.67 (0.25)
1.2	24.77 (1.29)	1.19 (0.02)	1.22 (0.02)	0.13 (0.03)	368 (106)	14.00 (0.23)
Mean	25.81 (1.52)	1.19 (0.02)	-	-	-	-

Table 4.1: Summary of SI at varying ϕ and constant $p_a = 1$. Values are represented as means with the SSD in parenthesis

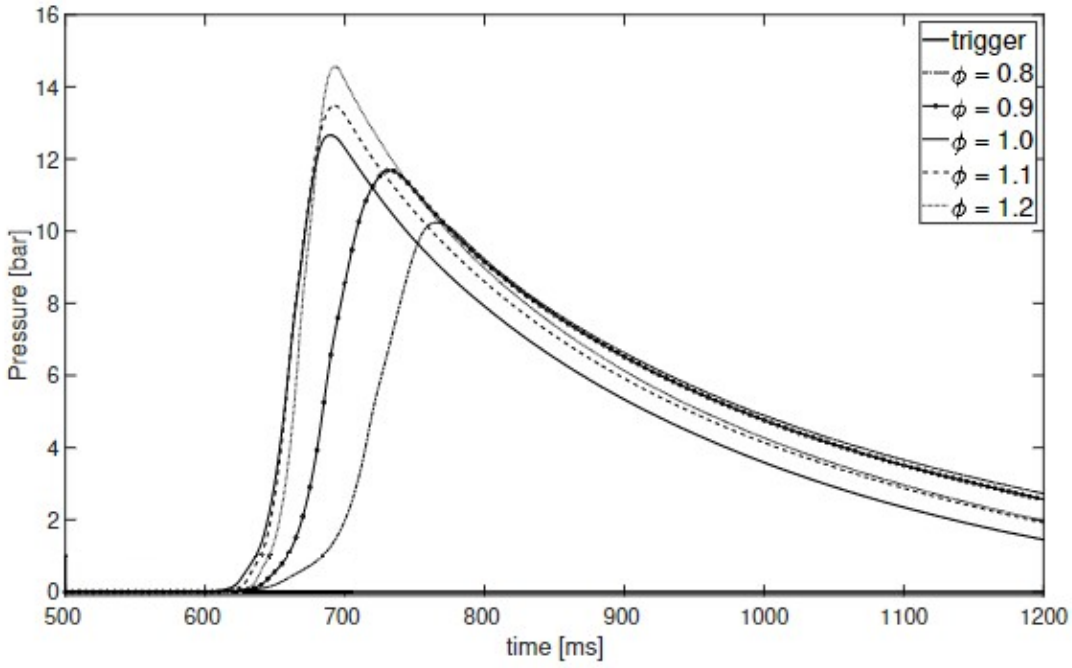

Figure 4.4: Combustion pressure development from SI with varying ϕ at $p_a = 1$ bar

Since the mixture composition was verified, Fig. 4.4 illustrates the pressure development for the cases in Tab. 4.1. The peak pressure had a close to linear relation with ϕ, with a maximum for $\phi = 1.2$. In terms of maximum pressure gradient and ignition delay, $\phi = 1.1$ yields the largest gradient and smallest delay which was to be expected due to the local maximum for the flame speed at $\phi = 1.1$. Stoichiometric mixture compositions had the shortest combustion duration and reached the peak pressure first, while $\phi = 0.8$ had the longest. Furthermore, for lean mixtures, the variation was larger, particularly for $\phi = 0.8$. p_{peak} has a 1.52 bar SSD, compared to $\phi = 1.0$ with 0.24 bar. The target was to do 15 experiments for each ϕ and while there was a 100 % success rate for $\phi \geq 1$, only about 30% of combustions at $\phi \leq 1.0$ led to ignition. $\phi = 1.0$ had all over less variations than the other tested ϕ.

The results from the investigation of the flammability limit for the chamber are listed in Tab. 4.2. The resulting flammability does not indicate consistent combustion, only that the mixture was able to ignite at those conditions at least once. The trend was that for the outer limits, the consistency of ignition significantly decreased. However, this consistency was not measured directly. The largest flammability limit was at the highest tested pressure at 4 bar, while the lowest on the lowest tested

p_a [bar]	Flammability limit [ϕ]
1	0.8-1.2
2	0.7-1.2
3	0.7-1.3
4	0.7-1.4

Table 4.2: Flammability limit of for CH_4 mixtures in the CVCC with SI

pressure at 1 bar.

To finalize the base study for SI, combustions for different p_a at constant $\phi = 1.0$ were examined and the pressure developments are listed in Fig. 4.5. The peak pressure increased linearly with an increase in p_a and the curves for 3 and 4 bar are in good proximity to each other regarding the ignition delay. Deviations started occurring for 2 bar and especially for the 1 bar curve which had a the greatest ignition delay.

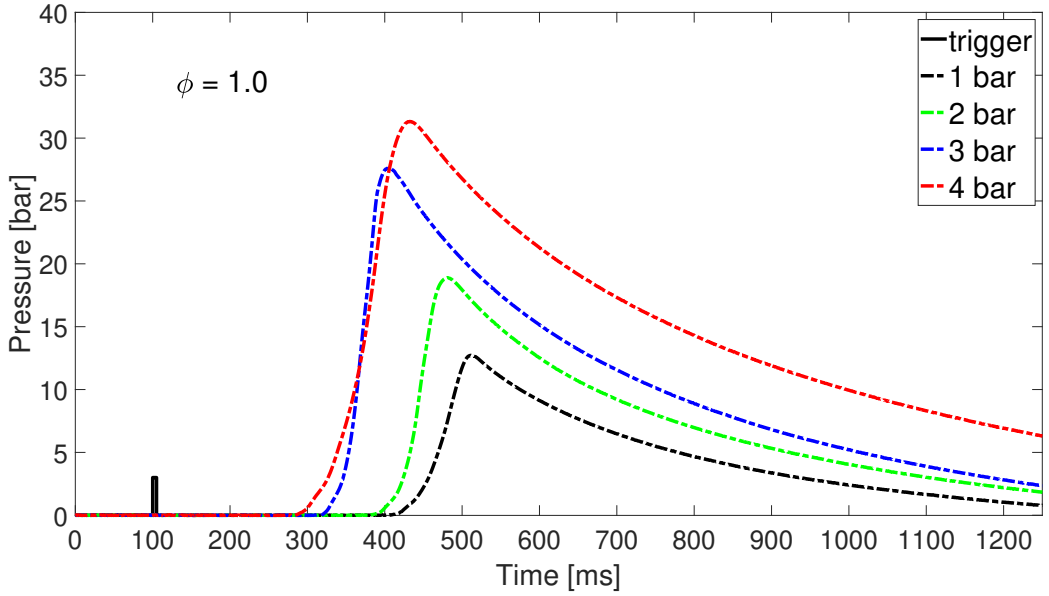

Figure 4.5: SI with varying initial pressures.

As for the overall statistics based on 120 samples, across the entire pressure and ϕ range, had an mean temperature on 24.8 (2.52)°C at the spark trigger. The SSD was approximately 1 °C larger than the isolated base case on $p_a = 1$. The maximum temperature across all combustions was at 33.75 ° while conducting safety tests for allowable pressures. While conducting tests at these pressures, a greater amount of condensation was observed in the chamber and especially around the spark-plug.

For the visual interpretation, the SI flame developments were filmed and the time lapse can be seen in Fig. 4.6. The columns represent the ϕ, from 0.9 on the left, 1.0 in the middle and 1.1 to the right. The rows shows the flame state at different time instances. Since the camera was not programmed for the spark trigger, the plots and figures are not synchronous. In the time lapse series, t = 0 corresponds approximately to the first time a kernel was observed. From this instance, intervals of 10 ms are included up until the flame takes off and the camera is not able to properly capture the mechanisms. Finally, a time instance at 200 ms was included to show the variations in the end gas.

$\phi = 0.9$	$\phi = 1.0$	$\phi = 1.1$
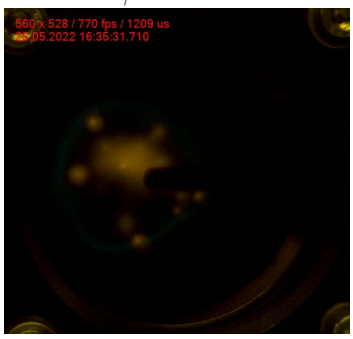		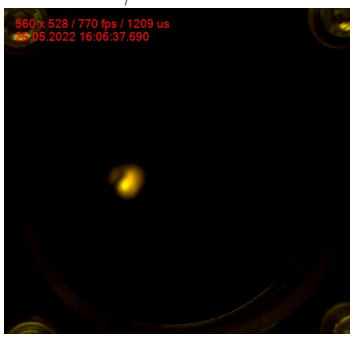
t = 0 ms		
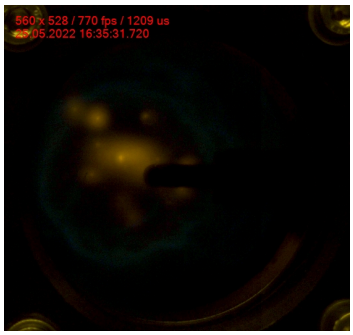	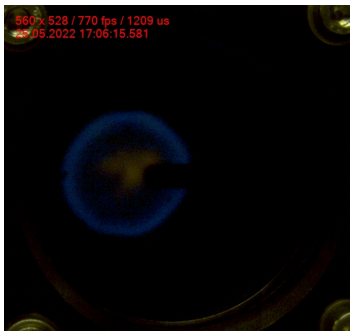	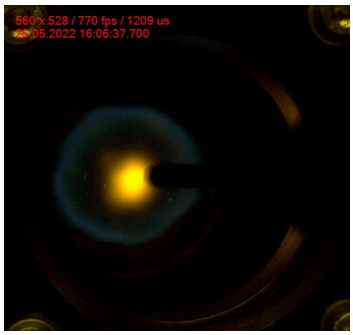
t = 10 ms		
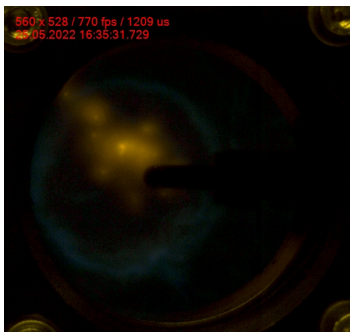	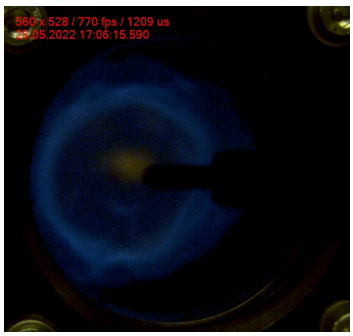	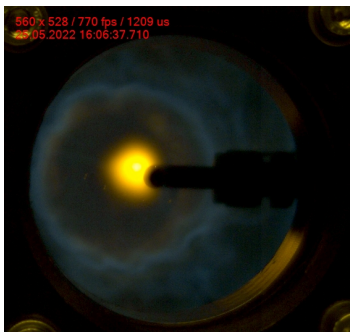
t = 20 ms		
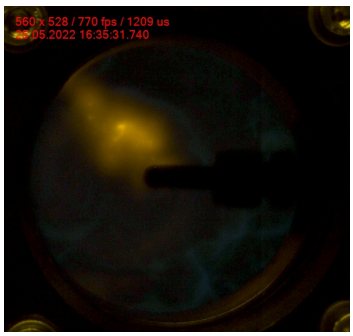	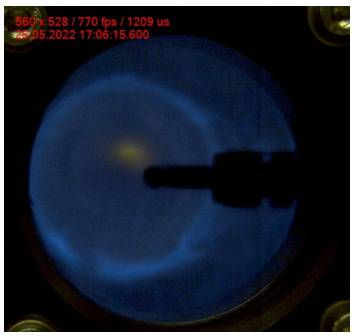	
t = 30 ms		

t = 40 ms

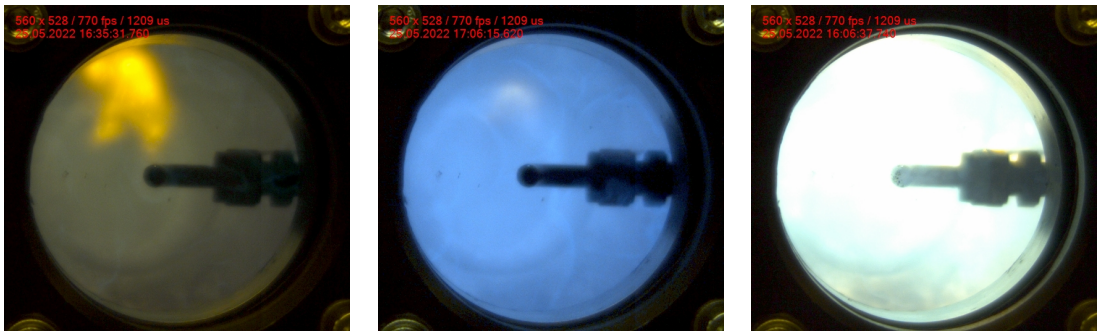

t = 50 ms

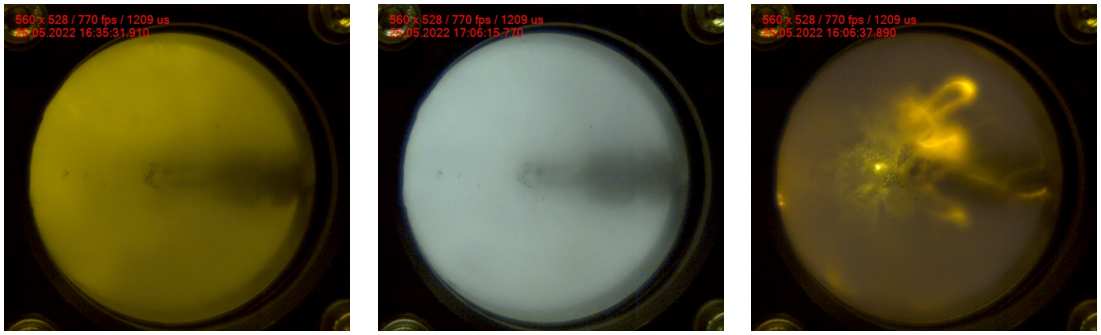

t = 200 ms

Figure 4.6: Flame development from SI with first kernel observation at t = 0 ms to t = 200 ms. Left column corresponds to $\phi = 0.9$, middle column is $\phi = 1.0$ and right column is $\phi = 1.1$

From the left column at $\phi = 0.9$, it looked like the combustion was significantly weaker than the two other cases. The combustion looked incomplete with a weak combustion wave and with local yellow points in the mixture. This could have indicated that for this combustion at $\phi = 0.9$, the charge was not properly premixed. For $\phi = 1.0$, the combustion seemed to be slightly fuel rich around the spark-plug, but as the combustion wave traversed the chamber, the blue colour dominated and the combustion looked complete. The final case for $\phi = 1.1$ had clear indications that

mixture was fuel rich. One can observe a bright yellow point around the spark-plug and blue colour from the combustion waves turning more yellow as time progresses. The end gas after 200 ms was dominated by after-burning and the combustion duration was increased.

Another time lapse for lean combustion was later on captured for comparison with PI. Figure. 4.7 shows the flame development at the elevated pressure of $p_a = 4$ bar and $\phi = 0.8$. This flame development was in better coherence with a complete combustion for a lean mixture, where all fuel is consumed.

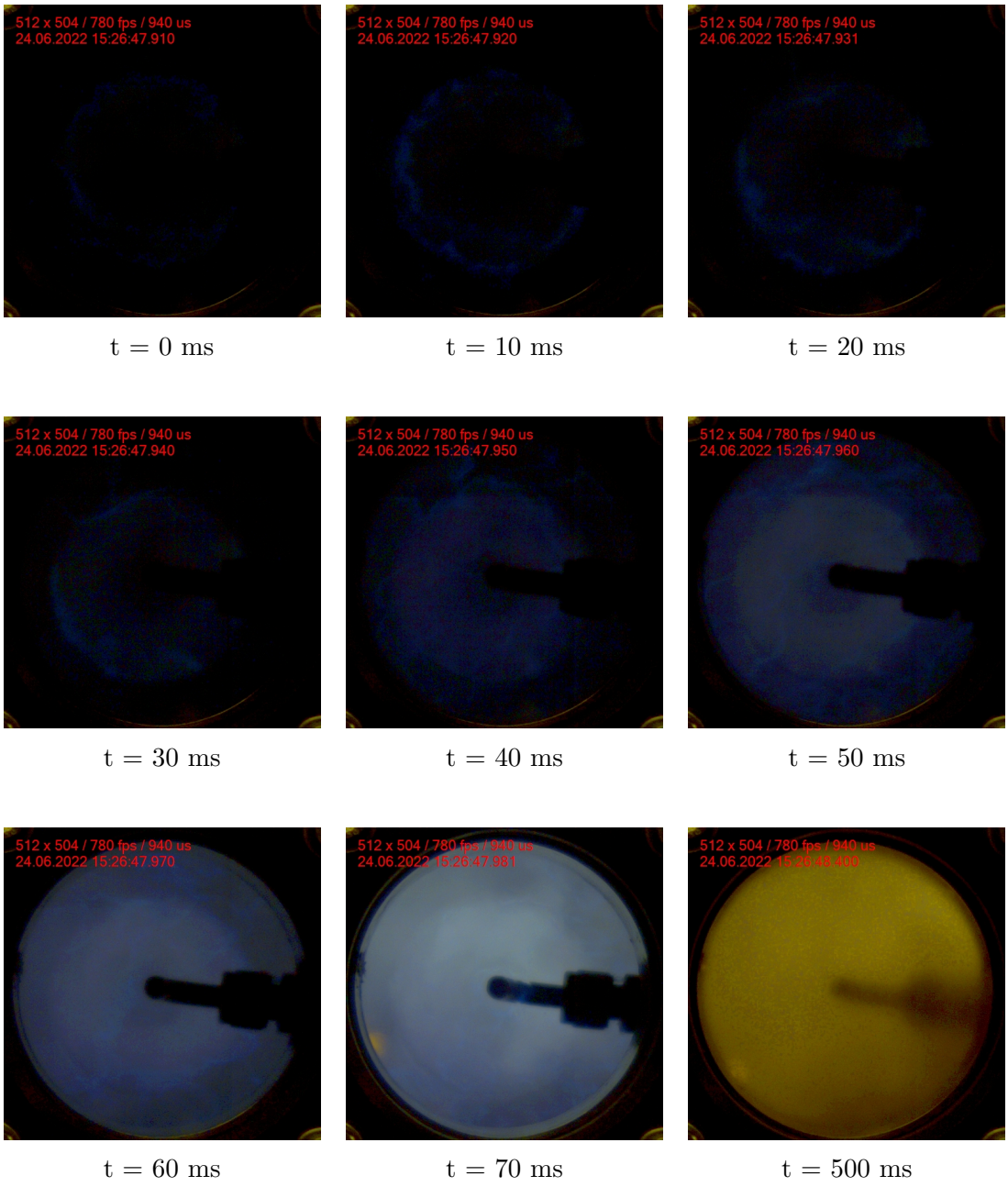

Figure 4.7: Flame development from SI with t = 0 ms slightly after trigger and intervals of 10 ms before the exhaust at t = 500 ms. Initial pressure at 4 bar and ϕ = 0.8

The base study came out to be reliable for all pre-combustion parameters. Most importantly, the ϕ_T was close to the real ϕ with an approximate 1-3% fuel-rich offset. This was a good results, considering that perfect coherence between the target and the actual value was not achievable when considering the sources of error. This was also an improvement of 20-40 % from last years study, mentioned in the previous work section 1.3. The deviations in that study were largest for low pressures, which seemed to have been resolved. The overall deviation on 1.5 °C from the target temperature at 25 °C was also satisfactory considering the challenges and required time to control this variable. The benefit of obtaining small temperature variations during the gas filling procedure was that the variations in the initial pressure was also kept low at 0.02 bar.

Regarding the combustion parameters, the results for varying ϕ was in good coherence with existing literature, with a local maximum on $\phi = 1.1$ for CH_4 in terms of pressure gradient and ignition delay. Maximum combustion pressure occurred at $\phi = 1.2$, where there was the most fuel to burn. Lean fuel mixtures had the longest ignition delay and the peak pressure had a linear relation with the initial pressure, as reported in [26]. Comparing the pressure dependence in Fig. 4.5 to the reference Fig. 2.3, it seemed that the different mixtures did not ignite at the same time during the spark trigger. This was particularly noticeable for the 1 bar case that yielded the longest ignition delay. Unfortunately, the spark trigger duration was not obtainable at this point so no further comment about this was made. The difference between the reference studies and this thesis was that the spark-plug was centered in the chamber, rather than mounted on the inner wall. Based on observations, it was assumed that the metal surface led to condensation of water vapor around the spark-plug gap, further increasing the effects of quenching and limiting kernel development. The delay seemed to be smaller in variations as the initial pressure rose, which could be explained by the low amount of fuel moles in the lower pressure range.

The combustion films for SI at 1 bar and varying ϕ in Fig. 2.2 gives a good indication that the flame was close to premixed, except for the lean case of $\phi = 0.9$. Comparing the time lapses of the fuel lean flames, where the first one was $p_a = 1$ bar at $\phi = 0.9$ and the later on was $p_a = 4$ bar and $\phi = 0.8$, it could be argued that the chamber was working unreliably at low initial pressures at lean mixture compositions. This was further enhanced by the narrow flammability limit and inconsistent ignition for the lean conditions. However, comparing the data at $p_a = 1$ bar with varying ϕ, the variations were as expected with the local maximum on the pressure gradient for $\phi = 1.1$, shortest combustion duration at $\phi = 1.0$ and slowest flame development for $\phi \leq 1.0$.

4.3 CNTs injection

In this section the results from the injection investigation is presented. The method applied is the method explained in section 3.4, where one large and one small injection tube, at 6 and 10 mm respectively, were tested. The target was three different Δp, but after doing injections with $\Delta p = 1$ bar it was observed that the pressure difference was not enough to carry all of the sample out of the pipes before equalizing the pressure. Ultimately, the consequence of having this Δp was that the solenoid valve got clogged by nano particles, having to replace it. Therefore, the rest of the injection test with both outlet pipes were done with $\Delta p = 2$ and 4 bar, and samples of 12, 24 and 36 mg with the 6 and 8 mm tubes.

First, looking at the 10 mm tube, it was evident that this tube was not suited for both tested Δp. The frame with most black pixels for this setup is shown in Fig. 4.8. Because of the larger diameter, hence a large pressure and lower velocity, the majority of the sample was attached to the center of the quartz glass. This led to the particles not being able to become dispersed nor detach from the window by gravity. As a consequence the chamber had to be opened after each injection and the 10 mm tube was neglected as a suitable injection tube.

Moving on to the 6 mm tube, which was the same diameter as the rest of pipes in the P&ID 3.6, this setup showed more promising results. Figure. 4.9 shows the results at the optimal frame at approximately 100 ms, with varying amount of CNTs at $\Delta p = 2$ bar. Only marginal differences were observed between 24 and 36 mg by the frame. However, the 36 mg sample tended to leave larger residues in the pipes and the solenoid valve, indicating that the current configuration did not efficiently transport the particles to the front of the quartz glass. It was decided that 24 mg should be the initial amount for PI testing.

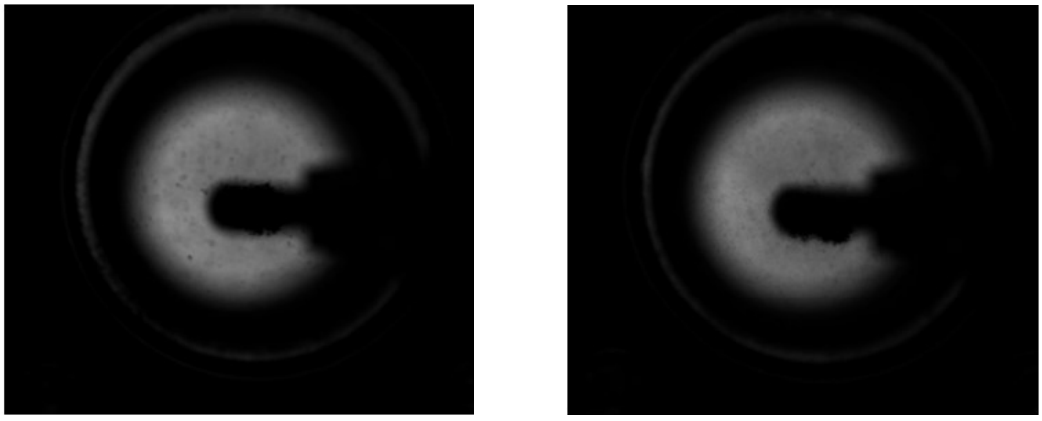

(a) $\Delta p = 2$ bar and 24 mg sample (b) $\Delta p = 4$ bar and 24 mg sample

Figure 4.8: Injection test for injection tube at 10 mm and 24 mg sample with varying Δp. Pictures at most dense frame

Initially it was decided that the particles should be injected with N_2 so that the fuel/oxidizer ratio remained constant. However, it was decided to make changes so that the injection gas could vary between N_2 and synair. The reason behind this was to create that local oxygen rich environment for the particles to ignite in, reported

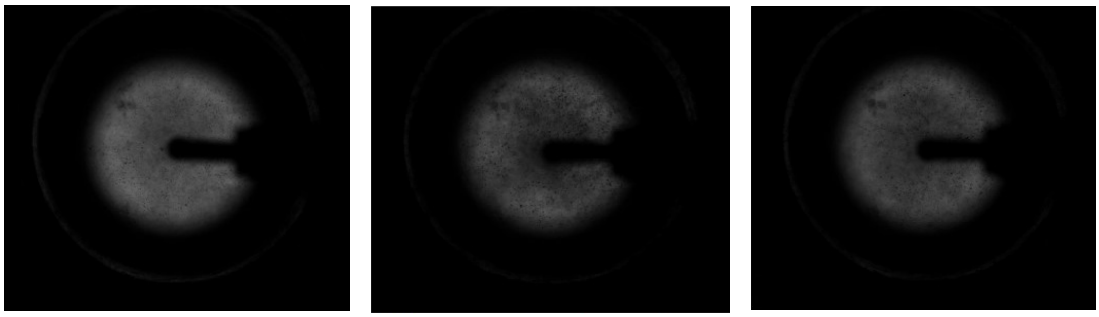

(a) 12 mg (b) 24 mg (c) 36 mg

Figure 4.9: CNTs injection with $\Delta p = 2$ bar and varying amounts of CNTs at most dense frame

by Cheroudi et al. [15] as a crucial component for successful ignition of fuel droplets. That being said, a limiting factor was that the synair supply pressure was capped at 5.5 bar, ultimately reducing Δp to a maximum of 1.5 bar while conducting tests for $p_a = 4$ bar. The change of strategy led to new injection tests, targeting $\Delta p = 1.5$ bar and the result is shown in Fig. 4.10. At t = 30 ms the particles exited the tube, while the optimal frame came out to be 113 ms after injection. It was also noticed that the particles appeared back in front of the window at around 205 ms, which made this time interesting with regards to PI. 113 and 205 ms was therefore suggested as the flash delay trigger time. As a final note, the pictures at $\Delta p = 2$ bar was denser than the $\Delta p = 1.5$ bar at the same amount. This meant that a greater amount of CNTs were not able to properly inject into the chamber at the lower tested pressure difference.

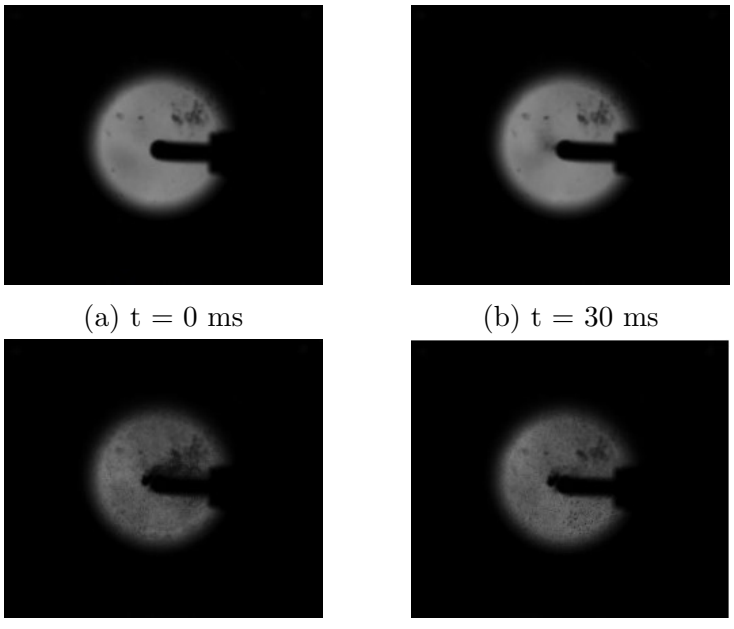

(a) t = 0 ms (b) t = 30 ms

(c) t = 113 ms (d) t = 205 ms

Figure 4.10: CNTs dispersion development with time. $\Delta p = 1.5$ and 24 mg sample

4.4 PI of CNTs

In this section the results from the method explained in section 3.5 is presented. Everything in this thesis up until this section was to support the chances of successful PI and the validity of the results. The PI experiments were conducted one time, before moving on to a new set of input parameters. The consequence of this investigative nature was that a mean or a SSD could not be calculated, hence no true conclusion could be drawn from the data in this section. That being said, to the best of this authors knowledge, successful PI of a combustible mixture from an externally mounted light source was for the first time initiated. The ignition method was also documented by filming the flame development in a different way than the reference studies to see the entire flame growth in a larger volume.

4.4.1 Chronological development of PI tests

The results in this section are presented chronologically as the experiments were conducted, leading up to the combination of factors that ultimately initiated the combustion. First, after developing the ignition strategy and setting up the `Godox` camera flash, several initial injection tests were performed. This was done to see if the injection strategy yielded any results and if the particles were able to ignite. Afterwards, a lot of burnt residue were found both quartz glass and in the chamber for all samples. This showed that the timing at $t_f = 113$ ms was able to ignite particles, but not the mixtures. Several other t_f, not validated through section 3.4 were blindly tested, ranging from 200 ms to 700 ms.

As injection did not yield any results, the next step was to move on to PI strategy number 1, static placement of the samples within the chamber. From here on out, the individual experiments are listed chronological in Tab. 4.3. Every sample was made "fluffy", as suggested as a key component for PI of CNTs by Ajayan et al. [1]. Experiment 1 to 13 covers the tests from this setup. The approach was to vary one of the parameters (p_a, ϕ, m_{CNT}, Fe wt%) while holding the others constant at the

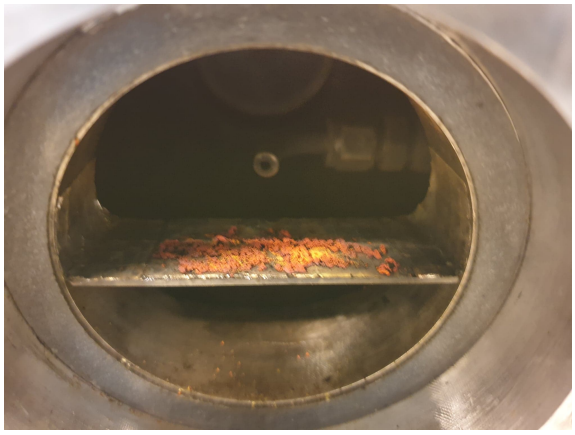

Figure 4.11: Typical result after static PI of CNTs particles within the chamber, 36 mg sample and Fe content of 66 wt%

value that yields the MIE or the highest energy output, see 2.1 and 2.2.4.

The majority of PI was performed with m_{CNT} = 12, 24 and 36 mg, but a small amount of 3 mg and a large amount of 96 mg were also subject to PI. From experiment 1 to 10 it was agreed that 3 bar should be the upper limit for the allowable pressure, but tests were carefully performed to see if this could further increase to decrease the MIE of the mixture. From experiment 11, 4 bar was the new upper limit.

From the static method, it was visually observed that every sample was subject to PI, but it was not enough to trigger the combustion of the mixture. The flame from the sample resembled a candle flame, non premixed and laminar by appearance. A lot of smoke and soot were observed for every attempt leaving a pile of CNTs with the outer layer being an orange like color from the oxidation of Fe. This is seen in Fig. 4.11. None of the aforementioned measures provided successful combustion of the mixture, excluding piling up CNTs in a combustible mixture as a potential strategy.

No.	Initial pressure [bar]	ϕ	Fe content [wt%]	Sample mass [mg]	PI strategy	Δp	Injection gas	Flash delay [ms]	Successful PI
1	3	1	33	24	Static (basket)	-	-	-	No
2	3	1	50	24	Static (basket)	-	-	-	No
3	3	1	66	24	Static (basket)	-	-	-	No
4	3	1	25	24	Static (basket)	-	-	-	No
5	3	1	70	24	Static (basket)	-	-	-	No
6	3	1	66	36	Static (glass plate)	-	-	-	No
7	3	1	66	24	Static (glass plate)	-	-	-	No
8	3	1	66	12	Static (glass plate)	-	-	-	No
9	3	0.8	66	24	Static (glass plate)	-	-	-	No
10	3	1.2	66	24	Static (glass plate)	-	-	-	No
11	4	1	66	24	Static (glass plate)	-	-	-	No
12	4	1	66	3	Static (glass plate)	-	-	-	No
13	4	1	66	96	Static (combined)	-	-	-	No
14	4	1	66	24	Dispersed	1.5	N_2	100	No
15	4	1.2	66	24	Dispersed	1.5	N_2	100	No
16	4	1	66	24	Dispersed	1.5	Synair	100	No
17	4	1	66	36	Dispersed	1.5	Synair	100	No
18	4	0.8	66	24	Dispersed	1.5	Synair	100	Yes
19	4	0.8	66	36	Dispersed	1.5	Synair	100	Yes
20	4	0.8	66	12	Dispersed	1.5	Synair	100	Yes
21	4	0.7	66	36	Dispersed	1.5	Synair	100	Yes
22	4	0.7	66	24	Dispersed	1.5	Synair	100	Yes
23	4	0.7	66	12	Dispersed	1.5	Synair	100	Yes
24	3	0.7	66	36	Dispersed	1.5	Synair	100	Yes
25	2	0.7	66	36	Dispersed	1.5	Synair	100	Yes
26	1	0.7	66	36	Dispersed	1.5	Synair	100	Yes
27	3	0.8	66	36	Dispersed	1.5	Synair	100	Yes
28	2	0.8	66	36	Dispersed	1.5	Synair	100	Yes
29	1	0.8	66	36	Dispersed	1.5	Synair	100	Yes
30	4	0.9	66	36	Dispersed	1.5	Synair	100	No
31	3	0.9	66	36	Dispersed	1.5	Synair	100	No
32	2	0.9	66	36	Dispersed	1.5	Synair	100	No
33	1	0.9	66	36	Dispersed	1.5	Synair	100	No
34	4	0.6	66	36	Dispersed	1.5	Synair	100	No
35	3	0.6	66	24	Dispersed	1.5	Synair	100	No
36	2	0.6	66	12	Dispersed	1.5	Synair	100	No
37	1	0.6	66	12	Dispersed	1.5	Synair	100	No
38	4	0.6	66	24	Dispersed	1.5	Synair	100	No
39	4	0.6	66	12	Dispersed	1.5	Synair	100	No
40	4	0.8	66	36	Dispersed	1.5	N_2	100	Yes
41	4	0.8	66	24	Injection	1.5	Synair	113	No
42	4	0.8	66	24	Injection	1.5	Synair	205	No

Table 4.3: Chronological development of PI tests, investigating the three PI strategies

Next up was the second PI strategy, listed in Tab. 4.3 as experiments number 14 to 40. Particles were laid out on the glass shelf before being dispersed by gas in front of the quartz glass. Then, after a constant t_f at 100 ms, the flash was initiated and particles ignited. This was done to simulate an injection in a very controllable environment. The first two attempts (No. 14-15) were done with $p_a = 4$ bar and $\phi = 1.0$ and 1.2 with N_2 gas. The particles ignited in a dispersed manner in front of the quartz glass, but no gas ignition was obtained. It was believed that it was the addition of N_2 that hindered the combustion, so the synair option was set up and tested for $\phi = 1.0$ with 24 and 36 mg without any success.

First successful PI was seen in experiment 18 and the remaining experiments up until 40 was to investigate limits with regards to p_a, ϕ and m_{CNT}. The only difference between experiment 17 and 18 was the ϕ being changed from 1.0 to 0.8. Therefore, the consecutive experiments were done with fuel lean mixtures with varying m_{CNT} and p_a. The result was a narrow flammability limit, from $\phi = 0.7$ to 0.8 at the p_a range from 2 to 4 bar. Within this range all tested samples from 12 to 36 mg successfully ignited the mixture. As for $\phi = 0.6$ a flame development was observed for $p_a = 3$ and 4, but extinguished before spreading into the majority of the chamber. The final experiment for this strategy was to change synair back to N_2 at ϕ to test out the assumption that particles had to be dispersed by synair. The mixture was able to combust similar to the experiments with synair.

The final two experiments were injection tests at lean conditions with the determined t_f at 113 ms and 205 ms. No combustion was achieved, indicating that the particle amount and distribution were not sufficiently similar to that of the successful cases. The only differences here was that the particles were transported through pipes, rather than being dispersed from a glass shelf.. Unfortunately, no further investigation of injection was feasible within the remaining time for this project.

4.4.2 Combustion trends with PI

As mentioned, each experiment was conducted once so no statistical foundation is laid out. However, it was interesting to observe the trend of the combustion pressure for the various combustions. Four plots were made to see the effects of varying p_a, ϕ, m_{CNT} and the injection gas.

Figure. 4.12 shows the variation of the combustion pressure at $m_{CNT} = 36$ mg and $\phi = 0.7$. As for this ignition method the peak pressure varies close to linearly with the initial pressure, where the peak is shifted forward in time as the initial pressure increases. The combustion seemed to trigger at the approximately same time, slightly after the 4.5 ms trigger. The figure is similar to that of the reference figure in Fig. 2.3.

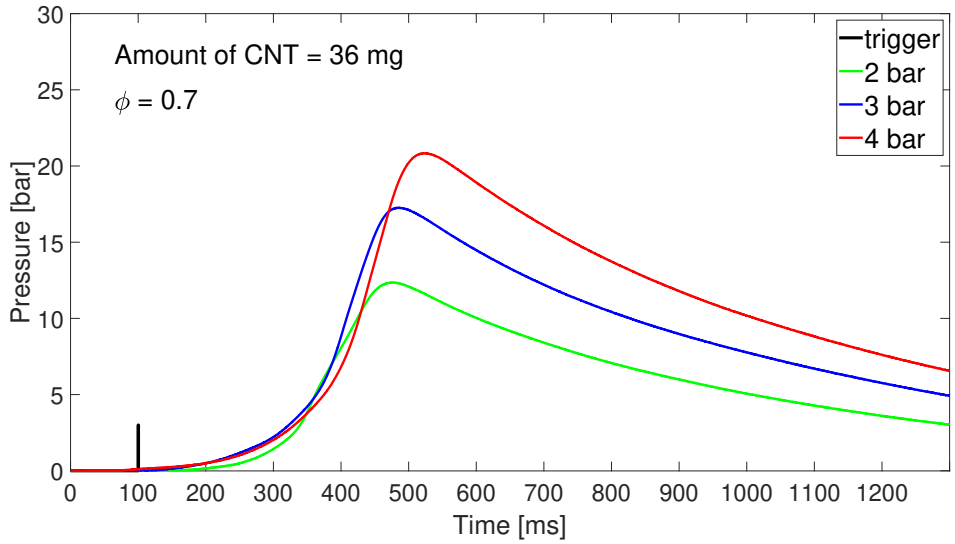

Figure 4.12: Pressure development from PI with different initial pressures at $\phi = 0.7$, $m_{CNT} = 24$ mg with Fe content at 66 wt%

Variation of amount at $\phi = 0.8$ and $p_a = 4$ bar is shown in Fig. 4.13 and compared to SI at the same inlet conditions. For the 12 mg sample, greater deviations from the other instances were observed as this had a longer ignition delay, lower pressure gradient and peak pressure. Based on the data, 24 mg had the fastest combustion, while 36 mg provided the largest peak pressure. However, 24 and 36 mg was too similar to both each other and to SI to say anything significant.

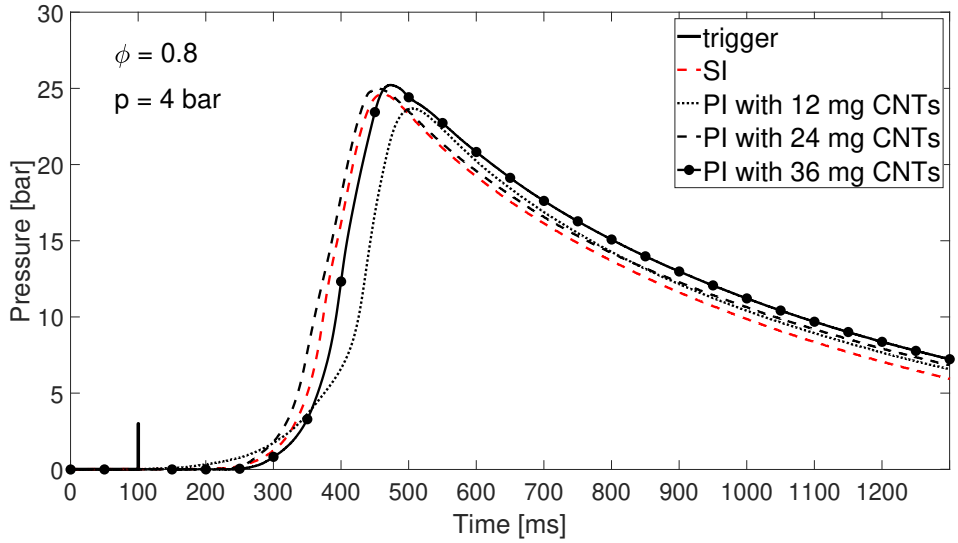

Figure 4.13: Pressure development from PI with different amounts of CNTs at $\phi = 0.8$, $p = 4$ bar and Fe content at 66 wt%

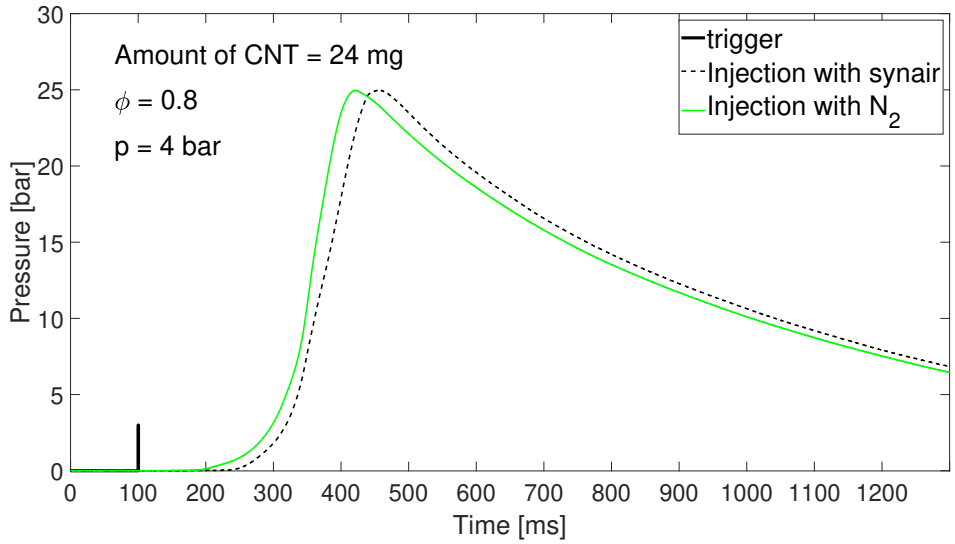

Figure 4.14: Pressure development from PI with different injection gases at $\phi = 0.8$, $m_{CNT} = 24$ mg and Fe content of 66 wt%

Figure. 4.14 shows the different pressure curves at $\phi = 0.8$, $m_{CNT} = 24$ mg and $p = 4$ bar, while dispersing the particles with either synair or N_2. The combustion data is so similar that the effects could not be differentiated.

The last figure, seen in Fig. 4.15, shows the variations between the two successful ϕ at 0.8 and 0.7 and also the pressure development for the case from $\phi = 0.6$. As expected, $\phi = 0.8$ yielded the most powerful combustion. For $\phi = 0.6$, the pressure built up to around 1.5 bar, before the flame extinguished.

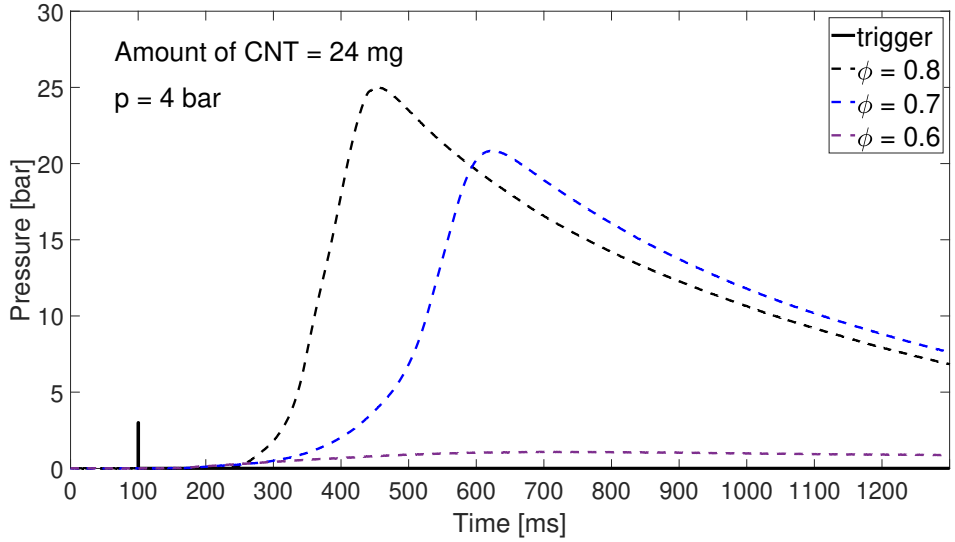

Figure 4.15: Pressure development from PI with varying ϕ at $p = 4$ bar, $m_{CNT} = 24$ mg and Fe content of 66 wt%

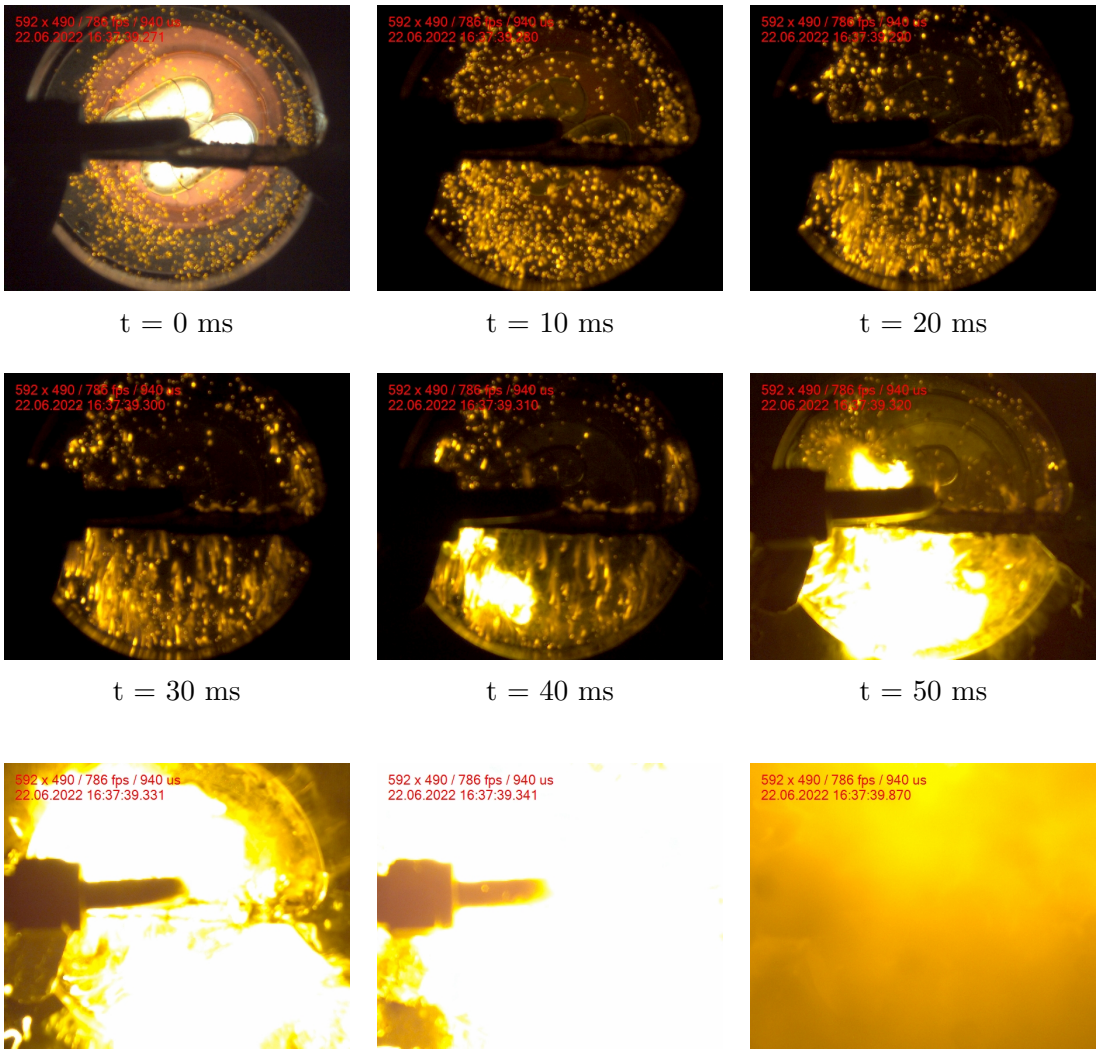

Figure 4.16: Flame development from PI at t = 0 ms after trigger and intervals of 10 ms before the end gas at t = 500 ms. Initial pressure at 4 bar, $\phi = 0.8$ and 36 mg of CNT with Fe content of 66 wt%

For filming the flame initiated by PI, Fig. 4.16 shows the development right after the flash trigger, defined as t = 0 s and frames are included in a 10 ms interval up to 70 ms. The burnt gas is shown at 500 ms. The particles were dispersed in front of the quartz glass in what looks like a close to uniform distribution. They were then exposed to the flash and then pulled downwards by gravity. At the frames between 20 and 40 ms, the particles seemed to gather in the down left corner, before having enough particles to reach the critical kernel size to initiate the combustion. The flame developed from what appeared to be 2 or 3 different locations. The flame, as well as the exhaust gas, was dominated by a bright yellow color, similar to the color of the particles before initiating the combustion of the mixture. Since the concept is so new and without much visual description, it would have been preferable to film every single experiment presented in this section. Unfortunately, the presented flame images marks the final experiment conducted in this thesis.

Going back to the CNTs injection strategy, the strategy developed did not bear any successful ignition. The developed method to analyze the particle distribution was a good approach to determine the flash trigger on a ms precision. However, the theory as of why the injection did not lead to PI was that the pipe diameter combined with the pipe-bend and a limited Δp led to not enough particles being carried out efficiently into the mixture. After injections, particles were found inside the pipes. From the flame development of a successful PI in Fig. 4.16 it looked like a substantial amount of burning particles had to come together to form a kernel beyond a critical size and the developed CNT injection strategy was not sufficient to deliver the right particle distribution to provide successful PI.

The static method showed very interesting results, even though no ignition was accomplished. From the first experiments, observing that an open flame was placed inside a combustible mixture, it was somewhat unusual to see that it did not trigger the combustion. All the efforts were put into keeping the MIE as low as possible while using the Fe content on 66 wt% to have the highest temperature output. However, after obtaining successful ignition it was evident that the MIE alone was not the issue. A reasonable explanation for the static case not being able to ignite the mixture could be that the burning of CNTs in a pile consumes too much of the local oxygen. Through the reactions of first Fe and the carbon in [2.2-2.4] the consumption of oxygen is present in every step. Moreover, considering the concentrated smoke in the dense samples, the products could hinder the CH_4/air mixture to get close enough to the high temperature zone in the flame which could initiate the combustion of the mixture.

The dispersed method that achieved ignition unambiguously achieved this for lean mixtures. Interestingly, the upper limit was $\phi = 0.8$ and the lower limit ϕ= 0.7. This underlines the aforementioned remark about oxygen deficits around the particles, where lean mixtures provide a higher content of oxygen relative to fuel. By reasoning, a lower amount of carbon and Fe could lead to less oxygen taking part in the local reactions which in turn consumes less oxygen around the flame kernel. On the other hand, the upper flammability limit were similar for all tested amounts. Optimizing the CNTs/Fe content with regards to minimum oxygen consumption, rather than maximum temperature output could be interesting to look at.

Since the successful PI experiments only were conducted once the uncertainty of the results are great. For the SI case, the largest SSD occurred at lean mixtures, adding an even greater uncertainty to the results. That being said, the pressure dependence in Fig. 4.12 is in very good coherence with the reference plot in Fig. 2.3. The pressures seems to evolve in a similar way to that of a SI, where the spark-plug was centered in the vessel. This further underlines the theory of the spark-plug not working optimally on low pressures and lean compositions. Observations for the varying amount in Fig. 4.13 indicated that the sample of 12 mg struggles more with the pressure rise than the other tested samples. This could mean that there were differences in amount of kernel growths, where the 24 and 36 mg samples evolved more rapidly from multiple points. Furthermore, the test between the injection gases showed similar trends where both successfully ignited the mixture. This undermined the initial theory that the particles had to be injected by an oxide.

The big differences between the flame development for SI and PI were because of the burning of CNTs and adding multiple ignition points. The CNTs became incandescent from the local heat, attributing the flame the bright, yellow color. The flame resembled a fuel rich flame, because of this dominating effect. However, this occur in the outer layer while the flame in general was lean. Looking at the reported black and white images by Berkowitz et al., the same trends were observed. The reported images were only captured 7 ms after the flash trigger so results are not directly comparable. As for Carlucci et al. , which performed the combustions in small cylinders, only the level of brightness was reported. The denominator between Berkwitz et al. and this study was that for both instances, a sufficiently large amount of burning particles had to come together in a dense area to form a flame kernel for the mixture to ignite. Therefore, the ignition delay of PI is strongly related to the burning particle distribution.

Combining the aforementioned argument with the overly dense particle distribution for the static case, there exist a set of burning particle densities which could lead to the ignition of a mixture. Too dense and the particle consumes all the local oxygen and too little would not release enough heat to reach the MIE of the mixture. The upper and lower particle density limits would probably depend on the CNT/Fe content as they consumes oxygen at a different ratio, but different compositions also release heat at a different rate. The amount and composition dependence should be further investigated to say anything with confidence.

Chapter 5

Summary

5.1 Conclusion

A CVCC has been utilized to investigate the combustion based on two different ignitions methods. The chamber was first verified in terms of SI for reliable operations, targeting a premixed low turbulent flame, before attempting PI of CNTs to ignite the mixture. Ultimately, a CH_4/air mixture was successfully ignited through the PI of CNTs, by an externally mounted Xe flash. The first steps were taken towards analyzing the flame development at different initial conditions by looking at pressure data and camera images.

A procedure was developed to ensure that the target mixture composition was in promixity to the real mixture composition. It was shown through a SI combustion study that the real equivalence ratio was at a 1-3% fuel rich offset from that of the targeted equivalence ratio. This was an improvement of about 20% compared to the project thesis. Furthermore, variations in the initial pressure and equivalence ratio did not have any significant correlations to the offset.

To target the homogeneous mixture composition, a fan driven by a magnetic stirrer was created through multiple 3D models being 3D printed and then tested in the chamber. The design that proved most consistent in terms of stability and reliability was a swirl generating fan, able to operate at 1200 rpm through many combustion cycles. To validate the premixed assumption, the flame development was filmed at different mixing times to visually determine the time where the mixture combusted without any locally fuel rich points. This occurred after 120 seconds of mixing. Moreover, the peak pressure variations created by the turbulence from the fan was investigated through varying the rotational speed. As expected, the highest rpm yielded the highest combustion pressure and to limit the effects of turbulence, the turbulence dissipation time was found to be 150 seconds.

With the set procedure to ensure a premixed low turbulent mixture, a SI combustion study was performed. The greatest flammability limit from SI of the mixture in the CVCC was found to be from $\phi = 0.7$ - 1.4 at the most elevated pressure at 4 bar. This is more narrow than the reference at 0.5 to 1.7 for atmospheric conditions

[27]. However, the reliability of the ignition in the chamber significantly improved compared to the initial study on the respective CVCC [6]. For the combustion characteristics, a local maximum in terms of maximum pressure gradient and minimum ignition delay was found at $\phi = 1.1$. The heat release rate was lowest for lean fuel mixtures having the slowest pressure rise time. The combustion peak pressure had a linear correlation with the initial pressures, with a maximum on 4 bar. The results were in good proximity with the reference studies [25], [26], [32], except for combustion at 1 bar. Ignition at this pressure seemed to have an extended ignition delay period, where combustion occurred at later time during the trigger than the other tested pressures.

For the PI of CNTs an injection method was developed and the particle distribution was analyzed through high speed camera images. It was found through image processing that the optimal flash trigger was 113 ms after initiating injection. The trigger time was then tested for PI of CNTs in a combustible mixture, where the particles ignited locally without initiating the combustion of the mixture.

Further investigation included placing the particles statically in the chamber while exposed to the flash. Open flames, which the size depended on the amount of particles were observed, but no successful ignition of the mixture was reported. The results yielded for pressures from 1 to 4 bar, amounts from 3 to 96 mg, ϕ from 0.8 to 1.2 and Fe content from 33 to 75 wt%.

The successful ignition occurred while dispersing the static sample in front of the quartz glass with a gas. The flame growth was located at the place where enough burning particles accumulated by gravity to form a kernel at the right size. The flame was bright and yellow from the incandescent of the added carbon, from the start to the end of the combustion process. Proper combustion occurred in the narrow lean range of $\phi = 0.7$ and 0.8 at all tested amounts and initial pressures from 2 to 4 bar. The combustion trends were plotted, but because of the narrow data-set no real comparison to SI was made, nor any conclusion from the combustion parameters could be drawn.

The key to achieving PI of a gas mixture in the explained configuration seemed to be the burning particle spacing rather than any other parameter. Static samples, piled in the chamber created an open flame and by doing so consuming the local oxygen around it. Injection did not obtain a dense enough particle distribution so the particles were not able to form a sufficiently large kernel and release enough heat to trigger the MIE of the mixture. Therefore, it could be argued that PI of CNTs in a combustible mixture is very dependent on the oxygen content of the mixture as well as the burning particle density and placing in the volume.

5.2 Further work

For the further work, the priority would be to replicate the PI experiments conducted one time to see the consistency in the results. A complete study on the combustion characteristics needs to be in place before comparing SI and PI to each other and the proposed reference studies for PI. The upper and lower limits of the ϕ and amounts of CNTs should be narrowed down to find the exact limit for when ignition occur.

Because of the lack of images of flame development by PI, tests at different initial conditions should be filmed and imagine processed. By filming the lower limit of particles that yields ignition a better understanding of the kernel growth could be obtained. By defining the required minimum and maximum particle density and its sensitivity, a larger leap towards integrating the ignition method in an engine cylinder could be made. After a more thoroughly analysis of the factors that provided ignition, injection should be reiterated to mimic these factors.

Finally, after achieving a better understanding of the concept the long term goal of igniting a NH_3/air mixture should be looked at. It would be interesting to see if the ignition method is more decisive on a fuel with more undesirable combustion characteristics than that of CH_4.

If the concept was to be put inside an engine, the Xe based flash is not feasible due to the charging time of the flash and durability. The flash would have to be replaced by a source that is able to flash at a high frequency and could withstand many cycles before breaking, such as LED. Moreover, a CNT injection system would need to be designed and optimized for engine applications. The issue regarding extensive soot formation in PI of CNTs would also need to be addressed.

Bibliography

[1] P. M. Ajayan, M. Terrones, A. de la Guardia *et al.*, 'Nanotubes in a flash–ignition and reconstruction', *Science*, vol. 296, no. 5568, pp. 705–705, 2002. DOI: 10.1126/science.296.5568.705.

[2] A. Berkowitz and M. Oehlschlaeger, 'The photo-induced ignition of quiescent ethylene/air mixtures containing suspended carbon nanotubes', *Proceedings of The Combustion Institute - PROC COMBUST INST*, vol. 33, pp. 3359–3366, Dec. 2011. DOI: 10.1016/j.proci.2010.07.013.

[Paris Agreement] *Paris agreement*, 2015. [Online]. Available: https://treaties.un.org/pages/ViewDetails.aspx?src=TREATY&mtdsg_no=XXVII-7-d&chapter=27&clang=_en (visited on 28th Mar. 2019).

[3] United Nations Environment Programme, 'Emissions gap report 2021: The heat is on – a world of climate promises not yet delivered', United Nations Environment Programme, 2021.

[4] International Maritime Organization. 'Fourth imo greenhouse gas study 2020'. (2020), [Online]. Available: https://www.imo.org/en/OurWork/Environment/Pages/Fourth-IMO-Greenhouse-Gas-Study-2020.aspx.

[5] X. Duan, M.-C. Lai, M. Jansons, G. Guo and J. Liu, 'A review of controlling strategies of the ignition timing and combustion phase in homogeneous charge compression ignition (hcci) engine', *Fuel*, vol. 285, p. 119 142, 2021, ISSN: 0016-2361. DOI: https://doi.org/10.1016/j.fuel.2020.119142. [Online]. Available: https://www.sciencedirect.com/science/article/pii/S0016236120321384.

[6] P. R.-F. H. Jørgensen, 'Combustion configuration for a constant volume chamber with sparkplug and photo ignition.', M.S. thesis, Norwegian Univeristy of Science and Technology, Høgskoleringen 1, 2021.

[7] S. R. Bratsberg, 'Photo ignition of carbon nanotubes with LED and laser diode', M.S. thesis, Norwegian Univeristy of Science and Technology, Høgskoleringen 1, 2021.

[8] A. P. Carlucci, P. Visconti, P. Primiceri, L. Strafella, A. Ficarella and D. Laforgia, 'Photo-induced ignition of different gaseous fuels using carbon nanotubes mixed with metal nanoparticles as ignitor agents', *Combustion Science and Technology*, vol. 189, no. 6, pp. 937–953, 2017. DOI: 10.1080/00102202.2016.1256880.

[9] A. P. Carlucci and L. Strafella, 'Air-methane mixture ignition with multi-walled carbon nanotubes (mwcnts) and comparison with spark ignition', *Energy Procedia*, vol. 82, pp. 915–920, Dec. 2015. DOI: 10.1016/j.egypro.2015.11.839.

[10] S. Rathinavel, K. Priyadharshini and D. Panda, 'A review on carbon nanotube: An overview of synthesis, properties, functionalization, characterization, and the application', *Materials Science and Engineering: B*, vol. 268, p. 115 095, 2021, ISSN: 0921-5107. DOI: https://doi.org/10.1016/j.mseb.2021.115095. [Online]. Available: https://www.sciencedirect.com/science/article/pii/S0921510721000556.

[11] N. Braidy, G. A. Botton and A. Adronov, 'Oxidation of fe nanoparticles embedded in single-walled carbon nanotubes by exposure to a bright flash of white light', *Nano Letters*, vol. 2, no. 11, pp. 1277–1280, 2002. DOI: 10.1021/nl025718m.

[12] N. N. Sysoev, A. I. Osipov, A. V. Uvarov and O. A. Kosichkin, 'Flash ignition of a carbon nanotube', *Moscow University Physics Bulletin*, vol. 5, no. 5, p. 492, 2011.

[13] J. Smits, B. Wincheski, M. Namkung, R. Crooks and R. Louie, 'Response of fe powder, purified and as-produced hipco single-walled carbon nanotubes to flash exposure', *Materials Science and Engineering: A*, vol. 358, pp. 384–389, Oct. 2003. DOI: 10.1016/S0921-5093(03)00282-X.

[14] S. H. Tseng, N. H. Tai, W. K. Hsu *et al.*, 'Ignition of carbon nanotubes using a photoflash', *Carbon*, vol. 45, no. 5, pp. 958–964, 2007, ISSN: 0008-6223. DOI: https://doi.org/10.1016/j.carbon.2006.12.033.

[15] B. Chehroudi, S. Danczyk, C. Morgan and A. Badakhshan, 'Ignition characteristics of single-walled carbon nanotubes (swcnts) utilizing a camera flash for distributed ignition of liquid sprays (preprint)', vol. 1, p. 8, Oct. 2008.

[16] S. Trewartha, R. Appleby, J. Gascooke and J. Shapter, 'Mechanism of laser initiated carbon nanotube ignition', *Propellants, Explosives, Pyrotechnics*, vol. 43, Jul. 2018. DOI: 10.1002/prep.201800023.

[17] B. Chehroudi, 'A novel distributed ignition method using single-wall carbon nanotubes (swcnts) and a low-power flash light', Jan. 2006.

[18] ——, 'On-demand activation of autoignition in hcci engines using distributed ignition of carbon nanotubes on-demand activation of autoignition in hcci engines using distributed ignition of carbon nanotubes', Jan. 2011. DOI: 10.13140/2.1.3549.0565.

[19] J. Warnatz, U. Maas and R. Dibble, *Combustion: Physical and Chemical Fundamentals, Modeling and Simulation, Experiments, Pollutant Formation*. Springer Berlin Heidelberg, 2012, ISBN: 9783642980282. [Online]. Available: https://books.google.fm/books?id=YuH1sgEACAAJ.

[20] W. W. Pulkrabek, *Engineering fundamentals of the internal combustion engine*, eng, Upper Saddle River, N.J, 2004.

[21] R. J. TABACZYNSKI, 'Turbulence and turbulent combustion in spark-ignition engines', in *Energy and Combustion Science*, N. CHIGIER, Ed., Pergamon, 1979, pp. 259–281, ISBN: 978-0-08-024780-9. DOI: https://doi.org/10.1016/B978-0-08-024780-9.50017-4. [Online]. Available: https://www.sciencedirect.com/science/article/pii/B9780080247809500174.

[22] M. Fathi, R. Khoshbakhti Saray and M. David Checkel, 'Detailed approach for apparent heat release analysis in hcci engines', *Fuel*, vol. 89, no. 9, pp. 2323–2330, 2010, ISSN: 0016-2361. DOI: https://doi.org/10.1016/j.fuel.2010.04.030. [Online]. Available: https://www.sciencedirect.com/science/article/pii/S0016236110002036.

[23] T. Badawy, X. Bao and H. Xu, 'Impact of spark plug gap on flame kernel propagation and engine performance', *Applied Energy*, vol. 191, pp. 311–327, 2017, ISSN: 0306-2619. DOI: https://doi.org/10.1016/j.apenergy.2017.01.059. [Online]. Available: https://www.sciencedirect.com/science/article/pii/S0306261917300673.

[24] M. Reyes, F. Tinaut, A. Horrillo and A. Lafuente, 'Experimental characterization of burning velocities of premixed methane-air and hydrogen-air mixtures in a constant volume combustion bomb at moderate pressure and temperature', *Applied Thermal Engineering*, vol. 130, Nov. 2017. DOI: 10.1016/j.applthermaleng.2017.10.165.

[25] G. Cui, W. Zeng, Z. Li, Y. Fu, H. Li and J. Chen, 'Experimental study of minimum ignition energy of methane/air mixtures at elevated temperatures and pressures', *Fuel*, vol. 175, pp. 257–263, 2016, ISSN: 0016-2361. DOI: https://doi.org/10.1016/j.fuel.2016.02.025. [Online]. Available: https://www.sciencedirect.com/science/article/pii/S0016236116001460.

[26] L. Huang, Y. Wang, S. Pei *et al.*, 'Effect of elevated pressure on the explosion and flammability limits of methane-air mixtures', *Energy*, vol. 186, p. 115 840, 2019, ISSN: 0360-5442. DOI: https://doi.org/10.1016/j.energy.2019.07.170. [Online]. Available: https://www.sciencedirect.com/science/article/pii/S0360544219315129.

[27] H. Kobayashi, A. Hayakawa, K. K. A. Somarathne and E. C. Okafor, 'Science and technology of ammonia combustion', *Proceedings of the Combustion Institute*, vol. 37, no. 1, pp. 109–133, 2019, ISSN: 1540-7489. DOI: https://doi.org/10.1016/j.proci.2018.09.029. [Online]. Available: https://www.sciencedirect.com/science/article/pii/S1540748918306345.

[28] R. S. Makepeace, 'The effect of turbulence on the combustion of gases', *Fire and Materials*, vol. 2, pp. 85–101, 1978.

[29] A. W. Date, 'Premixed flames', in *Analytic Combustion: With Thermodynamics, Chemical Kinetics and Mass Transfer*. Cambridge University Press, 2011, pp. 164–197. DOI: 10.1017/CBO9780511976759.009.

[30] J. Nakanishi, Y. Morimoto, I. Ogura *et al.*, 'Risk assessment of the carbon nanotube group: Risk assessment of cnt', *Risk Analysis*, vol. 35, May 2015. DOI: 10.1111/risa.12394.

[31] S. R. Bratsberg, 'Experimental investigation of carbon nanotube photo ignition for ammonia combustion in ICEs', M.S. thesis, Norwegian Univeristy of Science and Technology, Høgskoleringen 1, 2021.

[32] M. Reyes, F. Tinaut, A. Horrillo and A. Lafuente, 'Experimental characterization of burning velocities of premixed methane-air and hydrogen-air mixtures in a constant volume combustion bomb at moderate pressure and temperature', *Applied Thermal Engineering*, vol. 130, Nov. 2017. DOI: 10.1016/j.applthermaleng.2017.10.165.

Appendices

A Experimental configurations

This appendix contains the different experimental setups

A.1 Spark-plug setup

The following setup was used throughout the spark-plug combustions

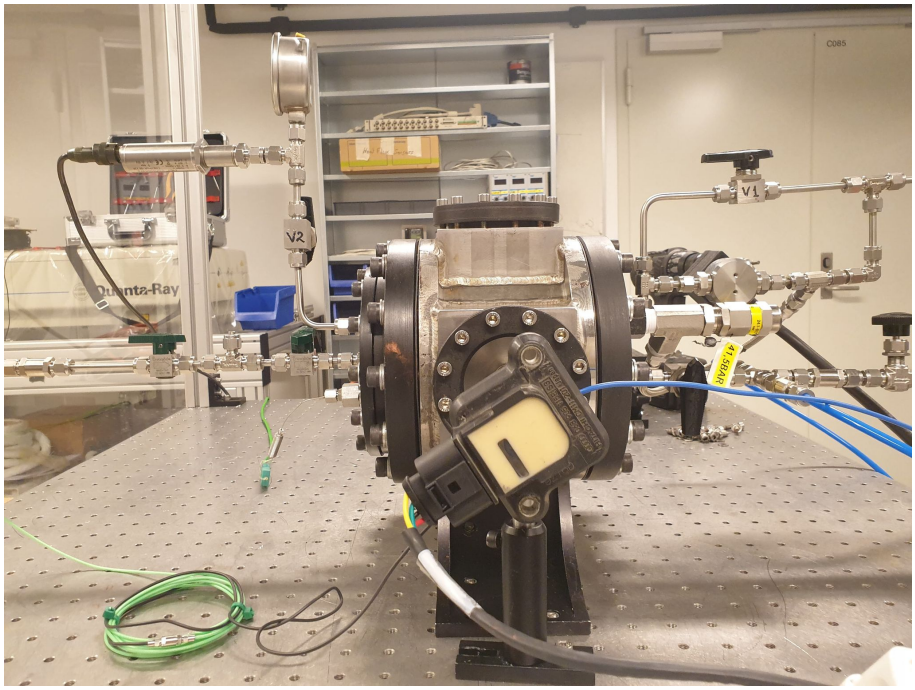

CVCC from the spark-plug side

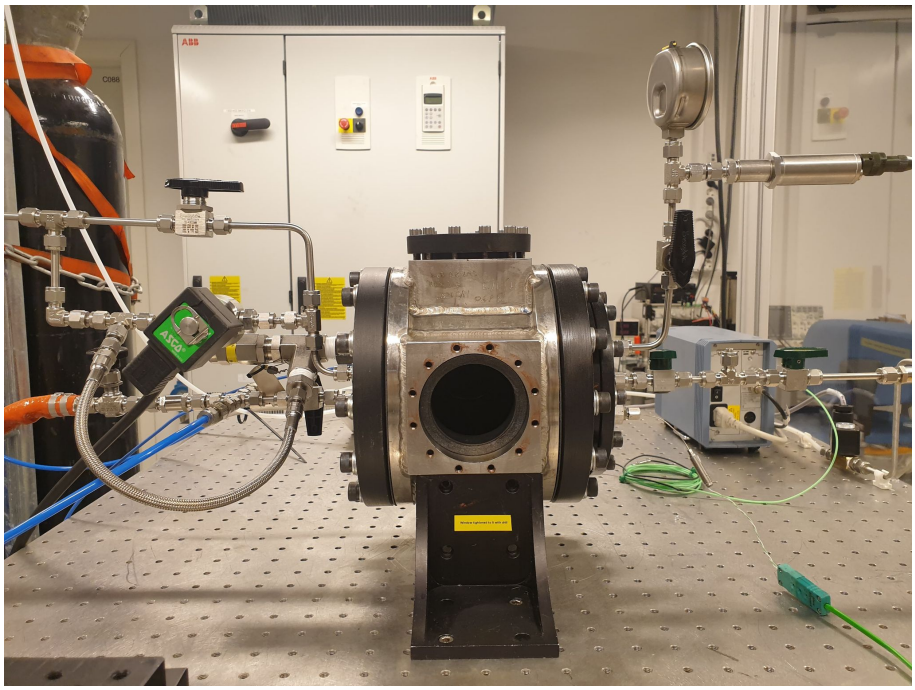

CVCC from the quartz glass side

Inside the chamber with a rotating fan on the bottom, the spark-plug in the right pocket and gas injection pipes

A.2 Fan designs

(a) 3D printed swirl fan

(b) 3D printed lift fan

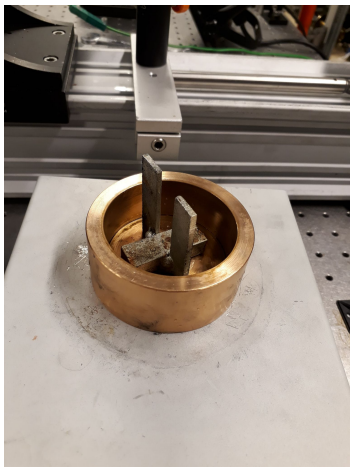

(c) Finalized design

Fan models that were tested during the design procedures, finalized design in picture c)

A.3 CNT injection setup

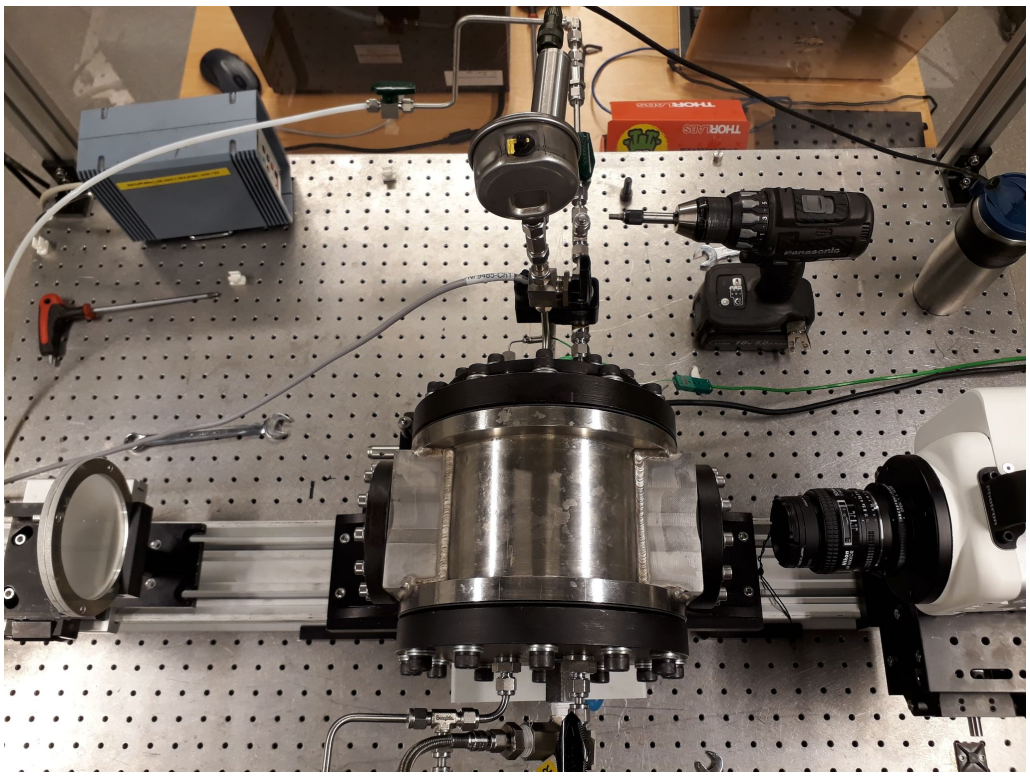

High speed camera setup with diffuser to investigate CNT injection strategies

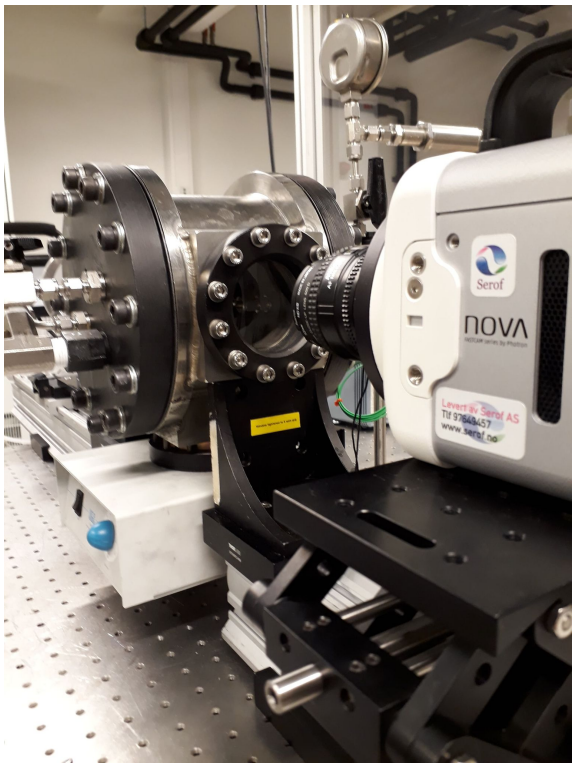

Side view of the high speed camera used during particle distribution analysis

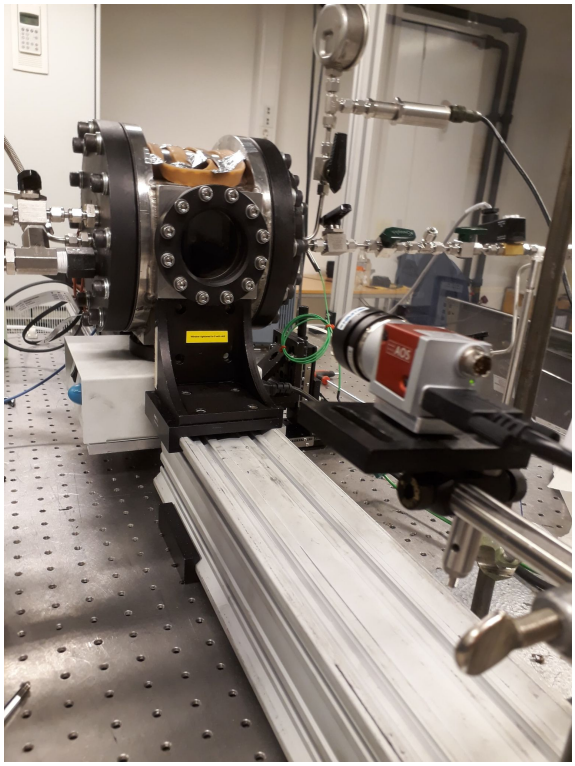

Side view for the lower speed camera used during PI

B Experimental deviations

Even though efforts have been made to reduce the overall error in this thesis, there are both some systematically and random errors occurring. The lab facilities are actively being used by others and the temperature is in general difficult to keep constant. The atmospheric pressure inside the lab facilities could vary based on the temperature, but is set as 1 bar throughout the thesis, which is the same as the software value. Regarding the systematical error the following measures have been made.

B.1 CNTs amount and Fe content

There are primarily two sources of error regarding the CNTs in this thesis, being the Fe content and the amount used in the experiments. As for the Fe content, a random amount of MWCNTs from `Nanografi` with 96% purity and diameters of 8 to 18 nm is sampled before being measured by `Sartorius Entris` analytical balance scale, which has a precision of 0.1 mg. Based on the weight of the sample and the given ratio, an amount of Fe from `Sigma Aldrich` is measured and mixed with the MWCNT.

Using the balance scale to measure every sample used in the combustion attempts would be very inefficient due to the HSE aspects of CNTs handling and it was therefore decided to a statistical analysis instead. 16 independent samples with 1:1 Fe/CNTs ratio were measured with a spoon and the results are listed in Tab. **??**.

No. of samples	Average	Min	Max	SSD
16	12.18 mg	8.20 mg	16.60 mg	2.41

Statistical analysis of amounts of CNT

B.2 Pressure calibration

The electrical manometer was calibrated using a `Fluke 729` automatic pressure calibrator with 0.01% precision. Since the pressure transducer has a 5 bar limit, calibrations for 0, 1, 2, 3 and 4 bar (gauge) were performed over a 60 seconds interval for each pressure while logging the voltage for each set. Furthermore, the voltage was plotted to determine the data distribution, then limited to a range to exclude outliers. The mean was calculated within that range with the SSD before relating the voltage and pressure through the proportionality given by Eq. B.2

$$p = 0.50V + 0.593$$

Where V is the measured voltage in volt and p the corresponding pressure in bar.

B.3 Filtering the data

By looking at the data it was evident that there are rarely any extreme outliers, but instead systematical oscillations. Therefore, to smooth out the data a moving average filter was used. This was particularly important to the pre-combustion curve as this data was chosen manually for calculating mixture composition. For the high speed pressure transducer, the data during the pressure rise is fairly free of noise. However, right after the ignition trigger the data was very noisy, to the point where the maximum value of the pressure gradient could be anywhere between the ignition trigger and the pressure rise. A typical example is shown in Fig. **??** where **??** shows the unfiltered data and **??** show the corresponding filtered data. .

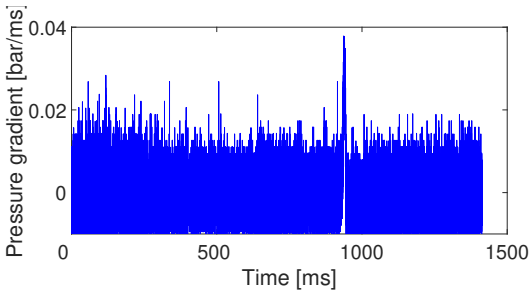

Unfiltered pressure gradient curve

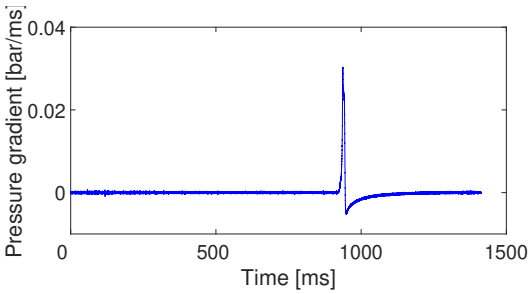

Filtered pressure gradient curve

Typical pressure gradient curve as a function of time for $p = 4$ bar, where the left figure is the unfiltered data and the right is the corresponding filtered

C Scripts

C.1 Optimal trigger code

```
clear all
clc

filename = 'test'; % Video file name
filetype = '.avi'; % Video file type

avgNumber = 5; % To filter out noice in image
numVideos = 1; % Number of videos
fps = 8000;    % Camera frame per second used to film the
    videos

% Preallocate memory
maximum = zeros(1,numVideos);
IND = maximum;
timing = IND;

%% Convert video to images and find image with most
   particles
for i = 1:numVideos
    v = VideoReader(strcat(strcat(filename,num2str(i)),
       filetype)); % Read video i
    j=1;
    while hasFrame(v) % Read frames as long as there is
       frames in the video
        frame = readFrame(v); % Read frame
        if j < 6

            % Find a background image the pixel values
               for the first
            % five images (before injection), in order to
                measure
            % change in pixel values
            background(j) = sum(sum(sum(frame)));

        else

            % Find the difference in pixel values between
                the current frame
            % and the average of the images before the
               injection
            sumCNT(j) = sum(sum(sum(frame)))/(sum(
               background)...
                /avgNumber);

        end
        j=j+1;
    end

    maximum(i) = min(sumCNT(avgNumber+1:end)); % Find
       frame with max pixels
    IND(i) = find(maximum(i) == sumCNT); % Find number of
        frame with max pixels
    timing(i) = 1000 * IND(i)/fps; % Optimum timing for
       flash [ms]
    storeImage = read(VideoReader(strcat(strcat(filename,
       num2str(i))...
        ,filetype)),IND(i)); % Read frame with max pixels
    imwrite(storeImage, [strcat(filename,num2str(i)) '.
       png']);  % Store frame with max pixels

    % Empty vectors
    sumCNT = [];
    background = [];
end
```

C.2 Data post-processing

```
clear all
clc
%% File and directory preparations
myDir = uigetdir;
Files = dir(fullfile(myDir));
Files_cell = struct2cell(Files);
file_path = Files_cell(2,3:end);
%File name spesification and formatting
file_name = string(Files_cell(1,3:end));
path_name = append(file_path,'\',file_name);
full_path = char(path_name);
filename_format_png = append(file_name,'.fig'); %Ensures
   that filenames ending with a format is saved as png

%% Mainloop, processing
k = 0; % counter
for k = 1:length(filename)
    %% TDMS reader
    TDMS_struct = TDMS_getStruct(full_path(:,:,k));

    %% Data extraction
    LS_time = TDMS_struct.Low_speed.Time.data;
    T = TDMS_struct.Low_speed.Chamber_temperature.data;
    P = TDMS_struct.Low_speed.Chamber_pressure.data;
    P_dyn = TDMS_struct.High_speed.Dynamic_pressure.data;
    HS_time = TDMS_struct.High_speed.HS_time.data;
    LS_datetime = datetime(LS_time, 'ConvertFrom', '
       datenum');
    %% Constants
    n = length(T);     %Array length for low speed excel
       sheet
    i = length(P_dyn); %Array length for high speed excel
        sheet

    %% Time formatting
    LS_datetime.Format = 'dd-MMM-yyyy';
    date = LS_datetime(1,1);
    LS_datetime.Format = 'hh:mm:ss.SSS';
    lowspeed_time = cellstr(LS_datetime);

    seconds_LS = zeros(n,1);

    for i=1:1:n
        seconds_LS(i)=sum(sscanf(lowspeed_time{i},'%f:%f
           :%f.fff').*[3600;60;1]);
    end

    % Make an array in format: 0:dt:end
    dt_lowspeed = diff(seconds_LS);
    t_cumulative_lowspeed = cumsum(dt_lowspeed);
    t_lowspeed = vertcat(0,t_cumulative_lowspeed);

    dt_highspeed = diff(HS_time);
    t_cumulative_highspeed = cumsum(dt_highspeed);
    t_highspeed = horzcat(0,t_cumulative_highspeed)
       ./10^6;

%% Filtering.

    %Formatting temperature array
    T_cutted = T(1:4:end);
    t_lowspeed_cutted = t_lowspeed(1:4:end);
    xq = 0:dt_lowspeed:length(t_lowspeed_cutted);
    T_interpolated = interp1(t_lowspeed_cutted,T_cutted);

    % Filter for dynamic pressure
    P_dyn_filtered = filtering(P_dyn,50);

    % Filter for static pressure
    P_filtered = filtering(P,10);
    %Storing variables
    P_max_filtered = max(P_dyn_filtered);
    dP = diff(P_dyn_filtered);
    dp = diff(P_dyn);
    P_max = max(P_dyn);
    T_max = max(T);
    T_min = min(T);
    dP_max = max(diff(P_dyn));
    dP_max_ind = find(dP==dP_max);
    T2 = max(T);
    P2_dyn = max(P_dyn);
    P2 = max(P);
end
```